

Mechanisms of Zanthoxyli Pericarpium-Zingiberis Rhizoma in the Treatment of Gastric Cancer Based on Network Pharmacology and Experimental Validation

Qian Gu¹, Shuai Duan¹, Joanna Japhet Tibenda¹, Boyun Gou¹, Shicong Huang¹, Guoqing Chen¹, Na Ning¹, Yuhua Du¹, Wenjing Liu², Yi Nan^{2,*}, Ling Yuan^{1,*}

¹College of Pharmacy, Ningxia Medical University, Yinchuan, Ningxia, People's Republic of China; ²Key Laboratory of Ningxia Ethnomedicine Modernization, Ministry of Education, Ningxia Medical University, Yinchuan, Ningxia, People's Republic of China

*These authors contributed equally to this work

Correspondence: Yi Nan, Key Laboratory of Ningxia Ethnomedicine Modernization, Ministry of Education, Ningxia Medical University, 1160 Shengli Street, Xingqing District, Yinchuan, Ningxia, 750004, People's Republic of China, Email 20080011@nxmu.edu.cn; Ling Yuan, College of Pharmacy, Ningxia Medical University, 1160 Shengli Street, Xingqing District, Yinchuan, Ningxia, 750004, People's Republic of China, Email 20080017@nxmu.edu.cn

Background: Malignant tumors, as a major challenge in global public health, have posed a significant threat to human life and health. Although traditional chemotherapy can inhibit tumor growth, it is often associated with serious adverse effects and tolerance. Against this background, Chinese medicine therapies have gradually gained wide recognition, and they play an important role in the treatment of gastric cancer (GC). As the core combination of the traditional prescription “Dajianzhong Tang”, the medicinal pair of Zanthoxyli Pericarpium and Zingiberis Rhizoma (ZP-ZR) has shown unique advantages in tumor treatment.

Purpose: To explore the mechanism of action of ZP-ZR in the treatment of GC using network pharmacology, bioinformatics analysis and in vitro experimental validation, and to provide a theoretical basis for subsequent experimental studies.

Patients and Methods: Subsequently, the effects of ZP-ZR on the proliferative ability of gastric cancer HGC-27 and AGS cell lines were verified by CCK-8, apoptosis, cycle and colony formation assays. The effects of ZP-ZR on the metastatic ability of GC cells were evaluated by Wound healing, transwell cell invasion and transwell cell migration assays. In addition, we evaluated the expression of Hub genes, pathway proteins and mRNAs by Western blot and qRT-PCR.

Results: ZP-ZR mainly regulated EGFR, PTGS2, MMP9, CXCL8, BCL2L1, CDK6, KIT target genes and PI3K/Akt pathway in GC for the treatment of gastric cancer. ZP-ZR inhibited the proliferation, induced apoptosis, blocked the cell cycle, and inhibited cell migration and invasion in AGS and HGC-27 cell lines. In addition, ZP-ZR affected the expression of PI3K-Akt-related proteins and decreased the mRNA expression of Hub genes.

Conclusion: ZP-ZR treats GC through the PI3K-Akt pathway. The present study provides a new idea for further investigation of ZP-ZR in the treatment of GC.

Keywords: zanthoxyli pericarpium-zingiberis rhizoma, gastric cancer, network pharmacology, molecular mechanism, in vitro experimental validation

Introduction

Gastric cancer is a malignant tumor originating from the epithelium of the gastric mucosa. Currently, gastric cancer stands as the fifth most common malignancy in incidence and the fourth in mortality, exerting a substantial impact on patients' quality of life.¹ It has been reported that the five-year survival rate exceeds 90% for early gastric cancer but falls below 30% for advanced cases, highlighting the need for effective treatment strategies.² At present, the primary treatment for gastric cancer is surgery, often accompanied by radiotherapy, chemotherapy and other comprehensive treatments.

However, these approaches frequently result in significant harm to the body. Despite radical surgery, 40–60% of patients experience recurrence and metastasis, leading to a poor prognosis.³ Radiotherapy and chemotherapy treatments often kill tumor cells while also damaging normal cells, causing side effects such as gastrointestinal issues, bone marrow suppression, and the hair loss, resulting in a poor overall prognosis for patients.⁴ Furthermore, with an increasing number of chemotherapy cycles, tumor cells exhibit decreased sensitivity to chemotherapeutic agents and develop resistance, ultimately leading to tumor relapse and metastasis, which adversely impacts treatment efficacy and long-term patient survival.⁵ There is an urgent need for a gastric cancer treatment that combines anti-cancer efficacy with mild side effects.

The Zanthoxyli Pericarpium-Zingiberis Rhizoma (ZP-ZR) combination, derived from Dajianzhong Tang in “The Essentials of the Golden Chamber”, includes Zanthoxyli Pericarpium, Zingiberis Rhizoma, ginseng, and cerealose. It has the functions of warming Yang and dispersing cold, tonifying deficiency and delaying urgency. It is a common prescription for clinical treatment of cold caused by deficiency of spleen and Yang. Zanthoxyli Pericarpium is the dried mature pericarp of *Zanthoxylum schinifolium* Sieb or *Z. bungeanum* Maxim of the Brassicaceae family.⁶ A number of national and international studies have shown that Zanthoxyli Pericarpium contains volatile oils, alkaloids, flavonoids, coumarin, lignan and many other different components, with analgesic, anti-inflammatory, antibacterial, antioxidant, anti-anxiety depression and other pharmacological effects.⁷ Meanwhile, recent studies indicate that Zanthoxyli Pericarpium and its active ingredients are effective in treating various cancers, including liver, stomach, and skin cancer. Zingiberis Rhizoma is the dried rhizome of (*Zingiber officinale* Rosc.) of Zingiberaceae, which is widely used in traditional Chinese medicine (TCM). Modern research shows that ginger mainly contains 6-gingerol, 6-shogaol and other components, contributing to its many biological activities, including antivomiting and antidiarrheal, anti-inflammatory and analgesic, hypolipidemia, hepatoprotective and choleric, anti-tumor and other pharmacological effects. Meanwhile, it has a protective effect on the cardiovascular and digestive systems,⁸ as well as improving the severity of nausea or vomiting after cancer chemotherapy.⁹ 6-shogaol, a component of Zingiberis Rhizoma that exerts anti-tumor effects, inhibits tumor cell growth and promotes cancer cell apoptosis.¹⁰ Furthermore, Zingiberis Rhizoma constituents influence cell cycle regulation, DNA damage response, epigenetic regulation and other processes, acting through specific cellular signaling pathways.¹¹ In clinical practice, Zingiberis Rhizoma is mainly used in combination with other medicines, which can enhance the therapeutic effect. Literature indicates that Dajianzhong Tang may inhibit gastric cancer progression by modulating MMP-9 expression via the ERK1/2 signaling pathway.¹² However, limited research exists on treating gastric cancer with ZP-ZR alone, and its mechanism of action remains unclear, which needs to be further investigated.

TCM has a long-standing history in China for cancer treatment and prevention, and is increasingly recognized for its synergistic effects and ability to reduce the toxicity of Western drugs. With the characteristics of multi-target and multi-component treatment of gastric cancer, TCM has great advantages in slowing down the development process of gastric cancer, improving patients' symptoms and prolonging the survival period, which is one of the hotspots in current research.¹³ Studies have demonstrated that the active ingredients and extracts in ZP-ZR inhibit gastric cancer cell proliferation, induce apoptosis, enhance the patient's immunity, and mitigate radiotherapy response. Volatile oil is an important component of Zanthoxyli Pericarpium, mainly found in Zanthoxyli Pericarpium fruits, where the main chemical components include alcohols, ketones, terpenes, olefins, esters, etc. It has certain analgesic, antibacterial and antitumor effects. Volatile oils from Zanthoxyli Pericarpium inhibit colitis mainly by modulating NF- κ B and PPAR γ channels, and also inhibit NLRP3 activation in colitis mice. This finding suggests a novel dietary approach for preventing ulcerative colitis.¹⁴ Meanwhile, the alkaloidal components in Zanthoxyli Pericarpium have biological activities such as anti-tumor, anti-inflammatory and analgesic.¹⁵ Selective JAKs inhibitors were found in total alkaloids extracted from Zanthoxyli Pericarpium, and Chelerythrine, as the most promising inhibitor of JAKs among the alkaloids, showed significant inhibitory effects on adhesion, migration, invasion, and apoptosis stimulation in AGS cells.¹⁶ Moreover, the extract of Zanthoxyli Pericarpium suppressed cell proliferation and triggered apoptosis through downregulation of Akt and MDM2 expression.¹⁷ Zingiberis Rhizoma extract and its main stimulating components, 6-gingerol and 6-shogaol, have been shown to have antiproliferative effects on several tumor cell lines.¹⁸ Relevant studies showed that 6-gingerol was able to affect caspase activation and PARP cleavage, thereby inducing apoptosis in colon cancer SW-480 cells and preventing tumor cell proliferation by inhibiting MAPK/AP-1 signaling.¹⁹ In a rat model of cisplatin-induced xenophagy,

6-gingerol exhibited potential antiemetic effects by suppressing the 5-HT_{3R}/Ca²⁺/CaMKII/ERK1/2 signaling pathway,²⁰ which ameliorated the symptoms of vomiting after chemotherapy in cancer patients. Meanwhile, Zingiberis Rhizoma has the effect of neutralizing gastric acid, which can reduce the stimulation of gastric acid on gastric mucosa, thus protecting the integrity of gastric mucosa. Its components, 6-gingerol and 6-shogaol, can stimulate gastric mucosa and pancreas, and promote the secretion of digestive juices, thus improving digestion.⁸ On this basis, this study further explored the mechanism of action of ZP-ZR in the treatment of gastric cancer.

The field of network pharmacology in Chinese medicine amalgamates systems bioinformatics, pharmacological principles, and computational analysis to explore the network-based biological foundations of complex diseases, Chinese medicine evidence, and herbal treatments, significantly contributing to the field's development.²¹ By constructing the “disease-gene-target-drug” interaction network, we have elucidated the influence of active drug components on disease networks and revealed the collaborative actions of these agents within the human body.²² This research strategy's holistic and systematic nature parallels the principles of diagnosing and treating diseases in Chinese medicine, emphasizing the multi-component, multi-pathway, and multi-target synergistic effects of TCM and its formulas. Network pharmacology is not only able to construct multilevel networks to realize the overall resolution of complex biological systems, but also able to increase the accuracy of target prediction by 35%-50% compared with traditional methods based on topological analysis and module identification, and at the same time, through the similarity analysis of disease modules.²³ Moreover, network pharmacology is often used in antitumor studies of traditional Chinese medicines. According to the relevant literature, 39 active ingredients from *Salvia miltiorrhiza* were identified, and these ingredients were predicted to target 544 genes related to colorectal cancer by network pharmacology. In vitro experiments demonstrated that *Salvia miltiorrhiza* effectively inhibited colorectal cancer progression by regulating the INS/SRC/IL6 pathway.²⁴ Network pharmacology provides a methodological bridge for the modernization of traditional Chinese medicine, and its “holistic, predictive, and verifiable” features perfectly fit the theoretical system of traditional Chinese medicine. Network pharmacology, a frontier in modern biomedicine, aligns with the need for systematic research methods in TCM. It integrates well with traditional practices and is anticipated bridging Chinese and Western medicine.²⁵ In the field of tumor therapy, Chinese medicine offers distinct advantages, such as promoting apoptosis, impeding metastasis and angiogenesis, overcoming multidrug resistance, modulating the immune response, and alleviating the toxic side effects associated with radiotherapy.²⁶ The pathogenesis of tumor-related diseases is very complex, and the use of network pharmacology to study tumors and their related herbal therapies can help us to understand and combat tumors in a more systematic and comprehensive way. Network pharmacology and molecular docking, which aligns with the holistic principles of TCM and its diagnostic and therapeutic approaches, offers a foundational reference for comprehensively understanding TCM's mechanisms in treating gastric cancer. Therefore, in this study, we predicted the potential targets of ZP-ZR against gastric cancer, constructed PPI network maps, performed Gene Ontology (GO) and Kyoto Encyclopedia of Genes and Genomes (KEGG) analyses. Apply clinical relevance analysis, gene mutation relationship, epigenetic regulation and repair analysis of damaged genes, immune infiltration analysis, and molecular docking validation for comprehensive evaluation. In addition, in vitro cellular experiments were performed to confirm the impact of ZP-ZR on gastric cancer cells, propose a potential mechanism underlying its therapeutic effect on gastric cancer, and establish a theoretical and scientific foundation for future research endeavors and clinical applications. The study's flowchart is illustrated in Figure 1.

Materials and Methods

Network Pharmacology Analysis

Acquisition of ZP-ZR Targets

The TCMSp database (<https://www.tcmsp-e.com/>) was used to search for the compounds of ZP-ZR, and the compounds were screened according to oral bioavailability (OB) \geq 30% and druglikeness (DL) \geq 0.18, identify the eligible candidates. The “Canonical SMILES” of each compound was obtained from PubChem database (<https://pubchem.ncbi.nlm.nih.gov/>), and the “Canonical SMILES” of each compound was transferred to Swiss ADME database (<http://www.swissadme.ch>) to test whether the compounds were active or not (GI absorption score was “high” and DL was screened by at least 2 “yes”).

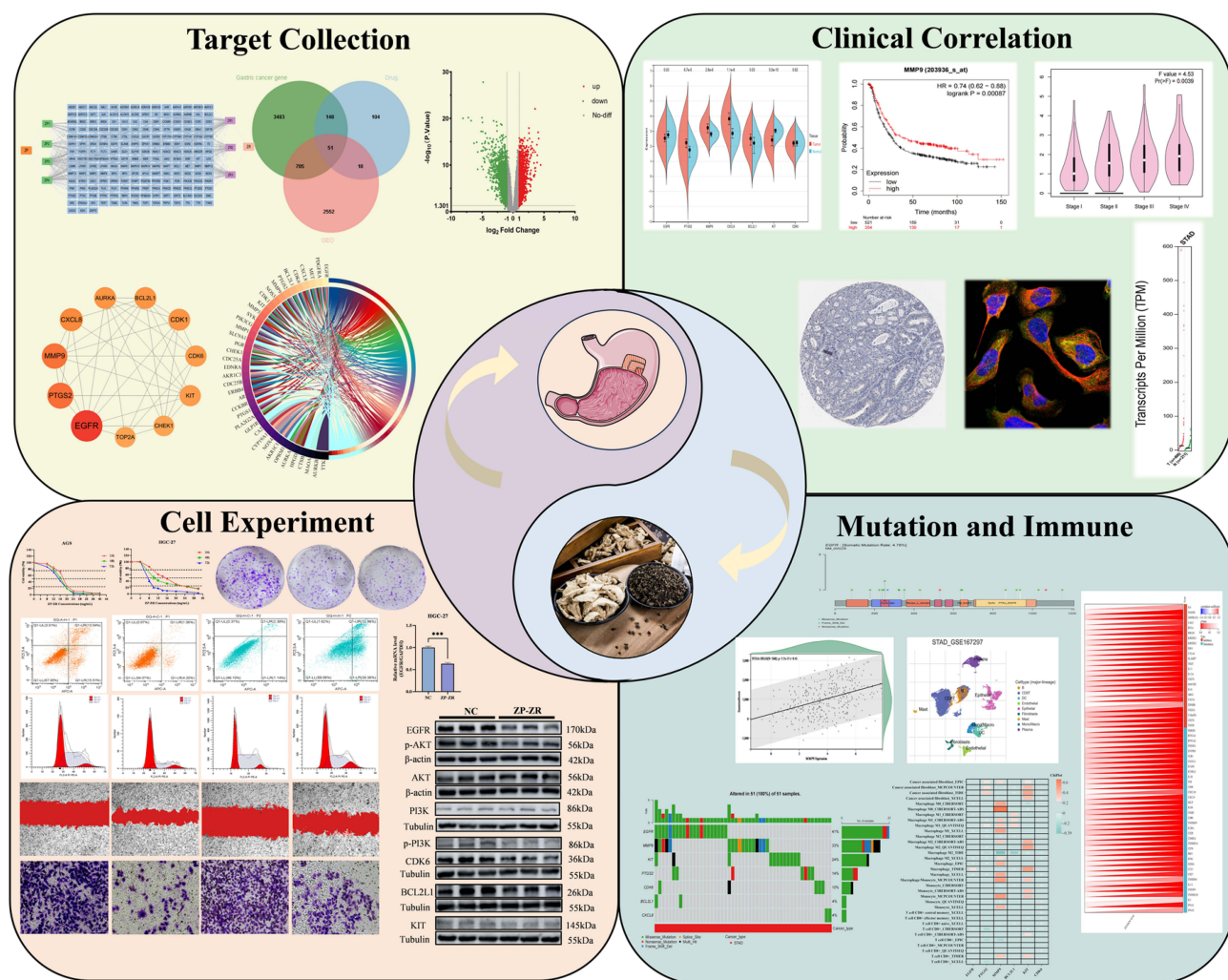


Figure 1 The flow chart of this study. *** $P < 0.001$.

The active ingredients were analyzed using its “Canonical SMILES” in the Swiss Target Prediction database (<http://swisstargetprediction.ch>) and the SEA database (<https://sea.bkslab.org/>) to find potential targets. After removing overlapping targets, the remaining targets were further examined to identify those associated with the drug ZP-ZR.

Gastric Cancer Target Acquisition and DEGs Screening

The Genecards database (<https://www.genecards.org/>), the OMIM database (<https://www.omim.org/>), and the DisGeNET database (<https://www.disgenet.org/>) were used to obtain relevant targets for the disease. Suitable gene chips were retrieved from the GEO database (<https://www.ncbi.nlm.nih.gov/>) database and screened for differentially expressed genes. Differential gene volcanoes were mapped using GraphPad Prism 9 software. The final intersection target was obtained by taking the intersection using the SRplot website (<http://www.bioinformatics.com.cn/>). Meanwhile, the SRplot website was used to draw equal scale Venn plots and heatmap display of the kurtosis values of the intersected targets. Meanwhile, in order to judge the quality of the selected samples, we performed PCA analysis on BioLadder website (<https://www.bioladder.cn/web/#/pro/index>).

Construction of Protein-Protein Interaction Networks and Screening of Potential Hub Genes

The overlapping targets were uploaded to the STRING 12.0 database (<https://cn.string-db.org/>) for the creation of a protein-protein interaction (PPI) network, and the findings were visualized. Utilizing CytoScape 3.10.0 software, potential core targets were filtered based on degree values, and a PPI network topology analysis map was generated.

GO and KEGG Enrichment Analysis

The intersecting targets were analyzed for GO and KEGG enrichment using the DAVID database (<https://david.ncifcrf.gov/tools.jsp>). The top 10 biological process (BP), molecular function (MF), cellular composition (CC) and top 20 KEGG signaling pathways were taken according to the Pvalue value to elucidate the key pathways of ZP-ZR against gastric cancer, respectively. According to the screening conditions for the gene ratio, Pvalue, and count value the results of enrichment analysis were visualized in the form of bubble diagrams using the SRplot website; the bigger the bubbles, the more the number of enriched genes; the redder the bubbles, the smaller the P-value, the more significant the function of the enriched genes. Biological pathway analysis was performed by the above GO and KEGG databases in order to elucidate the key pathways of ZP-ZR on gastric cancer.

KEGG Pathway and GSEA Analysis

The Hub genes were obtained by taking the intersection of the potential core targets with the genes in the pathway in the cancer pathway in the DAVID database. The pathway with the most significant correlation and more enriched genes was selected. Simplified KEGG pathway map was drawn by Adobe Illustrator 2022 software. The Hub genes were analyzed for GSEA enrichment using CAMOIP database (<http://www.camoip.net>).

Clinical Relevance and Prognostic Analysis

The expression levels of mRNA for Hub genes were retrieved from the Sangerbox database (<http://sangerbox.com>). Using the GEPIA database (<http://GEPIA.cancer-pku.cn/>), the correlation analysis between gastric cancer and adjacent tissues, as well as grading, staging, copy number, and survival prognosis analyses for Hub genes in gastric cancer, was conducted, and the results were visualized. Additionally, the protein expression levels of potential Hub genes were sourced from the UALCAN database (<https://ualcan.path.uab.edu/tutorial.html>). The expression levels of Hub genes in gastric cancer subtypes were obtained by GSCA database (<https://guolab.wchscu.cn/GSCA/>). Immunohistochemical expression maps of Hub genes in normal gastric tissues and gastric adenocarcinoma tissues were obtained by using HumanProteinAtlas database (<https://www.proteinatlas.org/>) by selecting TISSUE and PATHOLOGY, and immunofluorescence localization maps of Hub genes in tumor tissues were obtained by selecting SUBCELL. Survival curve maps of Hub genes were obtained by Kaplan-Meier Plotter database (<https://kmplot.com/>).

Impact of Hub Gene Mutations on Gastric Cancer

The GSCA database was utilized to obtain the mutation types and mutation sites of Hub genes in gastric cancer subtype. Additionally, a waterfall map of SNV mutation frequency of Hub genes and a bubble map of heterozygous and pure heterozygous CNV mutations was obtained. The CAMOIP database was used to analyze to obtain the mutational associations between driver genes and Hub genes in gastric cancer, as well as the MSI expression levels.

Hub Genes are Involved in Epigenetic Regulation and Repair of Damaged Genes

Methylation expression level profiles of Hub genes in normal and gastric cancer subtype groups were obtained by UALCAN database. The correlation of methylation levels of Hub genes with CTL markers in gastric cancer subtypes and survival curves of hypermethylated and hypomethylated subgroups was obtained by TIDE database (<http://tide.dfci.harvard.edu/>). Correlation was selected through GEPIA data, and the data of Hub genes with HRR and MMR repair systems were calculated separately, Excel tables were made, and ChiPlot (<https://www.chipplot.online>) was applied to draw the correlation heatmap.

Analysis of the Relationship Between Hub Genes and Immune Infiltration

Box plots were generated via the Sangerbox database after analyzing immune cells sourced from GEO probe files using the CIBERSORTx website (<https://cibersortx.stanford.edu/>). Stroma in the tumor tissue (StromalScore), immune cell infiltration in tumor tissue (ImmuneScore), and tumor purity (ESTIMATEScore) scatter plots of Hub genes associated with immune cells was obtained by selecting pan-cancer analysis in the Sangerbox database, respectively, and heatmaps of correlation between Hub genes and immune checkpoints were obtained. Single-cell sequencing maps with single-cell annotation maps in the Hub genes gastric cancer samples were obtained from the TISCH database ([Drug Design, Development and Therapy 2025:19](http://tisch.comp-</p></div><div data-bbox=)

genomics.org/). Data on the correlation of Hub genes with macrophage, endothelial cell, tumor-associated fibroblast, and CD8⁺ T cell infiltration were obtained using the TIMER2.0 database (<http://timer.cistrome.org/>).

Molecular Docking

The 3D structures of the core active ingredients of ZP-ZR and the 3D structure files of the Hub genes were downloaded. Sequential docking analysis was applied to obtain the blind docking scores of the Hub genes with the core active ingredients of the screened drugs using the CB-DOCK2 website (<https://cadd.labshare.cn/cb-dock2/php/index.php>) and the binding energy heatmaps were analyzed. Finally, PyMOL software was applied for visualization.

Experimental Verification

Cell Culture

Human gastric cancer cells AGS, HGC-27, and gastric mucosal epithelial cells GES-1 was purchased from Wuhan, China (Wuhan Pricella Biotechnology Co.,Ltd). The cells were cultured in an incubator environment at 37°C with 5% CO₂.

CCK8 Assay for Cell Viability

Trypsin was utilized to digest AGS cells, HGC-27 cells, and GES-1 cells that was in optimal growth condition, followed by their preparation into a cell suspension. A suspension of 6000 cells was added to 96-well plates. Once cells adhered and reached an optimal state, varying concentrations of ZP-ZR were introduced. The cells were incubated at 37°C for 24h, 48h and 72 h, with five replicates per group. 10uL of CCK-8 reagent were added to each 100uL of medium and co-incubated for 1 hour. The higher the number of live cells, the more products were generated and the darker the color. An enzyme marker was used to measure the OD of each well at 450 nm. The drug effect was indirectly assessed by calculating the cell viability from the OD value.

Apoptosis and Cycle Experiments

Apoptosis: 2×10^5 cells were inoculated in 6-well plates. Cells were collected after 24 hours of intervention by adding different concentrations of drug medium. According to the apoptosis assay kit instructions, Binding Buffer 500uL, Annexin V-FITC 5uL, Propidium Iodide 5uL were added sequentially, and the reaction was avoided from light for 5–15min, and then detected by flow cytometry within 1h. Three replicates were set up for each of the control, low, medium and high concentration groups.

The cell cycle process was similar to apoptosis experiments, with the difference that cell synchronization was induced by starvation for 6–8 hours after 80% cell fusion was observed under the microscope. After 24 hours of intervention with the addition of different concentrations of drug medium, cells were collected and fixed with anhydrous ethanol overnight. Afterwards, PI reagents and RNase were added and analyzed by flow cytometry according to the cell cycle assay kit instructions.

Clone Formation Experiment

Cells were inoculated in 6-well plates, and different concentrations of drug medium were added for intervention after the cells were in good condition. Cells were incubated at 37°C with 5% CO₂ for a duration of 7 to 10 days, with fresh medium replaced every 2 to 3 days. The culture process was concluded upon the appearance of visible cell clones (exceeding 50 cell clusters) on the 6-well plate. After fixation and staining, photos were taken for counting. Cells measuring 10 mm or larger were quantified using Image J software.

Wound Healing Experiment

Cells were inoculated in 6-well plates, and when the cell-adherent fusion reached about 90%, a scratch operation was carried out with the tip of a 10uL pipette gun. Each well was added with 2 mL of ZP-ZR medium containing different concentrations respectively, and photos were taken using a cell imager to record the photo position and observe the 0h scratch area. After 24h of incubation, the same scratch locations were photographed using a cell imager to observe and assess the wound healing ability.

Transwell Migration and Invasion Assay

Transwell migration: cells were collected and then resuspended using serum-free medium containing different concentrations of ZP-ZR and counted. A volume of 200 μ L of cell suspension was dispensed into the upper Transwell chamber, while 600 μ L of medium supplemented with 20% FBS was added to the lower chamber. Following incubation at 37°C for 24 hours in an incubator, the chambers, housed within 24-well plates, were fixed, stained, and photographed for cell counting purposes.

The procedure of Transwell invasion assay was similar to that of migration assay, and Matrigel gel was prepared with serum-free medium in the ratio of 1:15. Take 60ul of the prepared matrix gel and evenly apply it to the upper chamber of each Transwell, and leave it in the refrigerator at 4°C for 4–6 hours. The rest of the steps was consistent with Transwell migration. The information of specific experimental materials and reagents is shown in Table 1.

Quantitative Real Time Polymerase Chain Reaction (qRT-PCR)

Total RNA was isolated from the cells and converted into cDNA through reverse transcription. The gene expression was detected by reverse transcription quantitative PCR using the $2^{-\Delta\Delta CT}$ method. The primer sequences used are detailed in Table 2.

Western Blot

The total protein concentration was determined by using the BCA kit on the sample. Following electrophoresis and membrane transfer, the proteins were transferred to PVDF membranes. The PVDF membrane was sealed, and the respective primary antibody was introduced for overnight incubation at 4°C. Subsequent to washing, the corresponding secondary antibody was added and allowed to incubate at ambient temperature for 1.5 to 2 hours. Following exposure

Table 1 Experimental Materials and Reagents

Materials and Reagents	Manufacturer	Item Number
RPMI-1640	Invitrogen	IN0010
DME/F-12	Cytiva Corporation of the United States	SH30023.01
Fetal bovine serum	GEMINI	900108
PBS buffer	Cytiva Corporation of the United States	SH30256.01
Mixture of penicillin-streptomycin	Beijing solarbio Company	P1400
Trypsin - EDTA	Beijing solarbio Company	T1320
Matrigel	Biozellen Corporation of the United States	B-P-00002-10
4% polyformaldehyde fixing solution	Jinan century Tongda Chemical Co., LTD	30525-89-4
Crystal violet	Beijing Boaotoda Co., LTD	548-62-9
CCK-8 kit	KeyGEN BioTECH, China	KGA9305-500
Cell apoptosis detection kit	KeyGEN BioTECH, China	KGA106
Cell cycle test kit	KeyGEN BioTECH, China	KGA512
Trizol reagent	ThermoFisher Scientific of the United States	343,706
PrimeScript RT kit	Takara, Japan	RR047A
SYBR Premix Ex Taq TM II kit	Takara, Japan	RR820A
Whole Cell Lysis Assay	KeyGEN BioTECH, China	KGB5303-50
BCA Protein Quantitation Assay	KeyGEN BioTECH, China	KGB2101-50

Table 2 qRT-PCR Primer Sequence Information

Genes	Forward	Reverse
EGFR	TCGGCACGGTGTATAAGGGACTC	ACGGTGGAGGTGAGGCAGATG
PTGS2	GGGTTGCTGGTGGTAGGAATGTTC	CTGCCTGCTCTGGTCAATGGAAG
MMP9	CTGGTCTGGTGCTCCTGGTG	CTGCCTGTCGGTGAGATTGGTTC
CXCL8	GGACCACACTGCGCCAACAC	CCCTCTGCACCCAGTTTTCTTG
BCL2LI	GAGCTGGTGGTTGACTTTCTC	TCCATCTCCGATTCAAGTCCCT
KIT	GCGGACGAGATTAGGCTGTATG	CGGTGTTGGTGGCTTCTGC
CDK6	CCGAAGTCTTGCTCCAGTCCAG	GGGAAGGGCAACATCTCTAGGC
GAPDH	CAGGAGGCATTGCTGATGAT	GAAGGCTGGGGCTCATT

Table 3 Experimental Antibody Information

Antibody	Manufacturer	Article Number
EGFR	Abmart	T55112F
KIT	Abways	CY5359
PI3K	Affinity	AF621
p-PI3K	Affinity	AF3241
Akt	Affinity	AF6261
p-Akt	Affinity	AF0016
CDK6	CST	Cat. No. 3136
BCL2LI	MCE	HY-P80566

and image capture, the gray values of the protein bands were analyzed using Image J software. The specific primary antibody information is shown in [Table 3](#).

Statistical Analysis

All reactions were performed in triplicate (n=3). All data were statistically analyzed using GraphPad prism 9 software and expressed as mean \pm standard deviation. Statistical differences were analyzed using one-way ANOVA and *t*-test, **P* < 0.05, ***P* < 0.01, ****P* < 0.001.

Results

Network Pharmacology Analysis results

Screening of ZP-ZR Targets

Seven active ingredients of ZP-ZR were screened from TCMSP database and Swiss ADME database (Detailed information on the active ingredients can be found in [Supplementary Table 1](#)). The Canonical SMILES of the active ingredients in ZP-ZR were retrieved from the PubChem database, the targets were predicted and de-duplicated to obtain 321 drug targets. A “drug-ingredient-target” network diagram was generated using Cytoscape 3.10.0 software ([Figure 2A](#)).

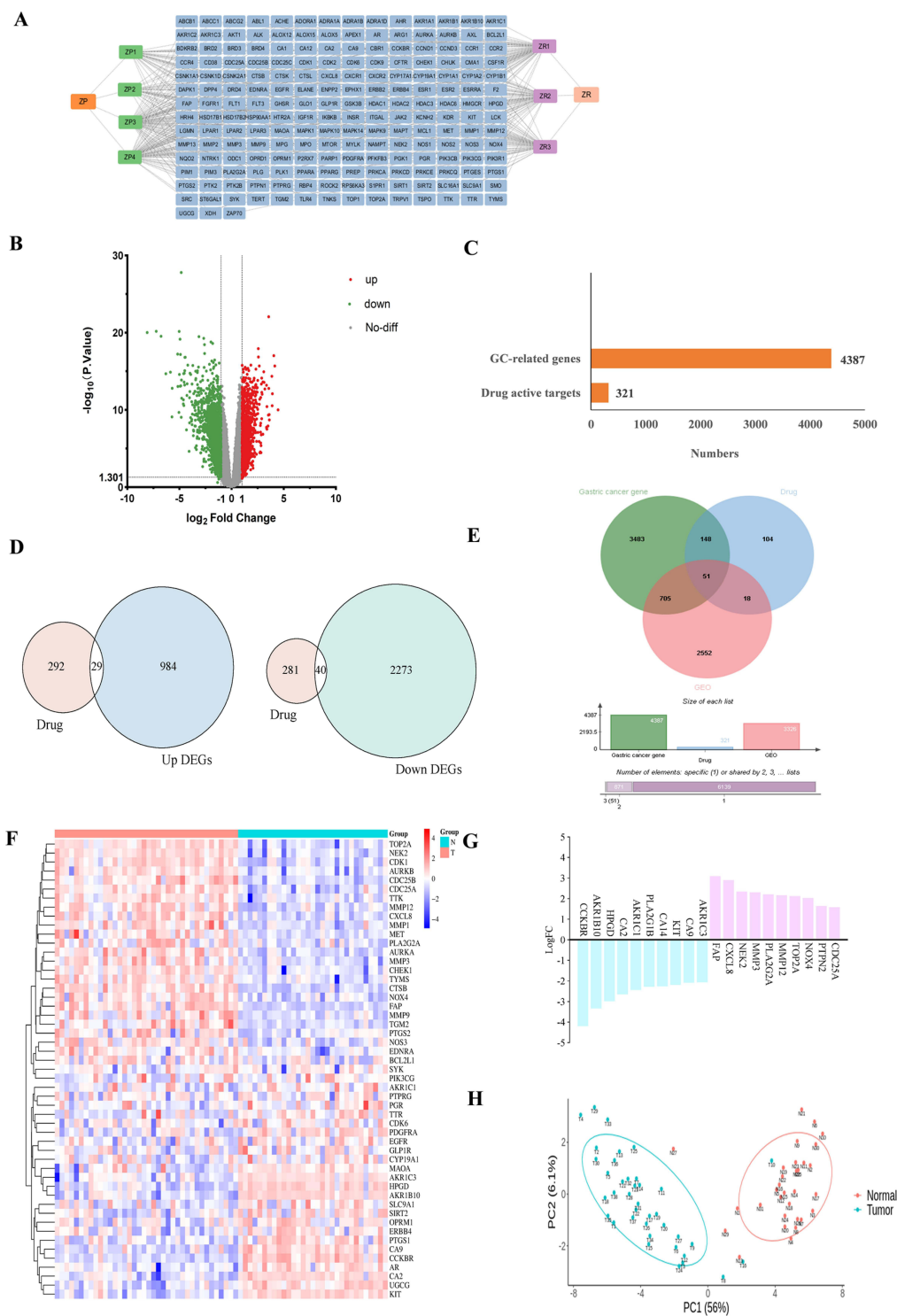


Figure 2 Targets of ZP and ZR active ingredients and differentially expressed genes in gastric cancer **(A)** Network diagram of ZP and ZR active ingredient-targets. Green and purple colors represent ZP and ZR, respectively, and blue color represents all the targets of active ingredients. **(B)** Volcano plot of differentially expressed genes of GSE13911. Where green represents down-regulated genes, red represents up-regulated genes, and gray indicates no difference or no significance. **(C)** All genes of gastric cancer and the number of targets of ZP and ZR active ingredients. **(D)** Intersection of up- and down-regulated genes of gastric cancer and targets of ZP and ZR. The pink color represents the targets of the compound, and the blue and green colors represent the up- and down-regulated genes, respectively. **(E)** Intersection plot of ZP and ZR and gastric cancer targets. Green and pink represent Genecards and GEO datasets, respectively, and blue represents ZP and ZR. **(F)** Heatmap of intersecting targets. Pink and green represent the tumor group and normal group, respectively. **(G)** LogFC values of the top 10 up- and down-regulated genes in the intersection targets, where red and blue represent up- and down-regulated genes, respectively. **(H)** PCoA plots of the samples of the intersecting targets. Red dots represent normal group samples and green dots represent tumor group samples.

Screening of Gastric Cancer Targets

The GEO database, created by the NCBI, is a public resource for high-throughput gene expression and genomics research, featuring extensive data from tumor and normal tissue gene chips.²⁷ The GSE13911 GeneChip dataset was selected in the GEO database to predict gastric cancer targets, and 3326 differentially expressed genes were finally obtained and the differentially expressed gene volcano plot was drawn (Figure 2B). The green, red and gray dots in the volcano plot represent down-regulated genes, up-regulated genes and genes with no differences, respectively. To compensate for the possible limitations of GEO data alone, 4,387 disease targets were obtained. After removing overlapping gastric cancer targets obtained from GeneCard, OMIM and DisGeNET databases, and drug-disease target bar graphs were plotted (Figure 2C).

Acquisition of Target Genes at the Intersection of ZP-ZR and Gastric Cancer

The targets of ZP-ZR were intersected with up-regulated and down-regulated genes, with 29 and 40 intersections, respectively, and an equal-scale Venn diagram was drawn (Figure 2D). The intersection of differential genes of gastric cancer, gastric cancer targets and the targets of ZP-ZR were taken, and a total of 51 intersecting target genes were obtained, and the Venn diagrams and cluster heatmaps were plotted (Figure 2E and F), and the heatmaps showed that the kurtosis values of the intersecting targets had a good distribution, and most of the targets were low-expressed in the normal cells and high-expressed in the tumor cells. Bar graphs were plotted for the top 10 up- and down-regulated target genes with LogFC values, respectively (Figure 2G). By PCA analysis, it was found that the aggregation within groups was better and there was no intersection between groups, indicating a better sample representation of the selected targets (Figure 2H).

Construction of Interaction Networks Between Target Proteins and Screening of Core Targets

A PPI network analysis was conducted for 51 intersection target genes, comprising 51 nodes and 216 edges, including 4 unconnected target genes. The network was imported into Cytoscape software, where the unconnected genes were removed, resulting in 47 associated target genes. By iteratively filtering based on the median degree value, 11 potential core targets were identified, which may represent the Hub genes of ZP-ZR in the treatment of gastric cancer. The degree values of these Hub genes decreased progressively, with nodes decreasing in size and transitioning in color from red to yellow (Figure 3A). And the 11 potential Hub genes were distributed in a bar graph based on the degree values (Figure 3B). Analysis of the correlation heatmap between potential core targets revealed that there was a better synergy between core targets, and the darker the color indicated a stronger correlation (Figure 3C).

GO Biological Function and KEGG Enrichment Analysis

GO functional enrichment analysis was conducted on 51 intersection genes, yielding 557 BP entries, 35 CC entries, and 54 MF entries. The entries with the top 10 P value values were screened separately to draw bubble diagrams (Figure 3D), where the circle size corresponds to the number of enriched targets, with larger circles indicating more enriched targets. Subsequently, KEGG analysis was applied to the same 51 genes, yielding 60 associated pathways depicted in a string diagram (Figure 3E). The pathways with the top 15 P value values were screened to draw Sankey diagrams (Figure 3F), where the left side represents the cross-targets, the center displays the pathways, and the curves represent their relationships. On the far right, a bubble diagram displays the KEGG results, where larger and redder circles indicate more significant pathway enrichment. The findings primarily associate with pathways in cancer and the PI3K/Akt signaling pathway.

Hub Gene Screening and GSEA Analysis

In the KEGG pathway bubble map, the pathway with the most significant correlation is “Pathway in cancer”, and more target genes were enriched, which is mainly involved in apoptosis and inhibition of tumor angiogenesis. The 11 potential core targets were intersected with the targets enriched from the “Pathway in cancer” to obtain the final 7 hub genes, namely EGFR, PTGS2, MMP9, CXCL8, BCL2L1, KIT, CDK6. Meanwhile, the pathway with the second most significant correlation was the PI3K/Akt signaling pathway, which was shown in detail (Figure 4A), the red color indicates up-regulated genes and the blue color indicates down-regulated genes. It was found that four Hub genes were

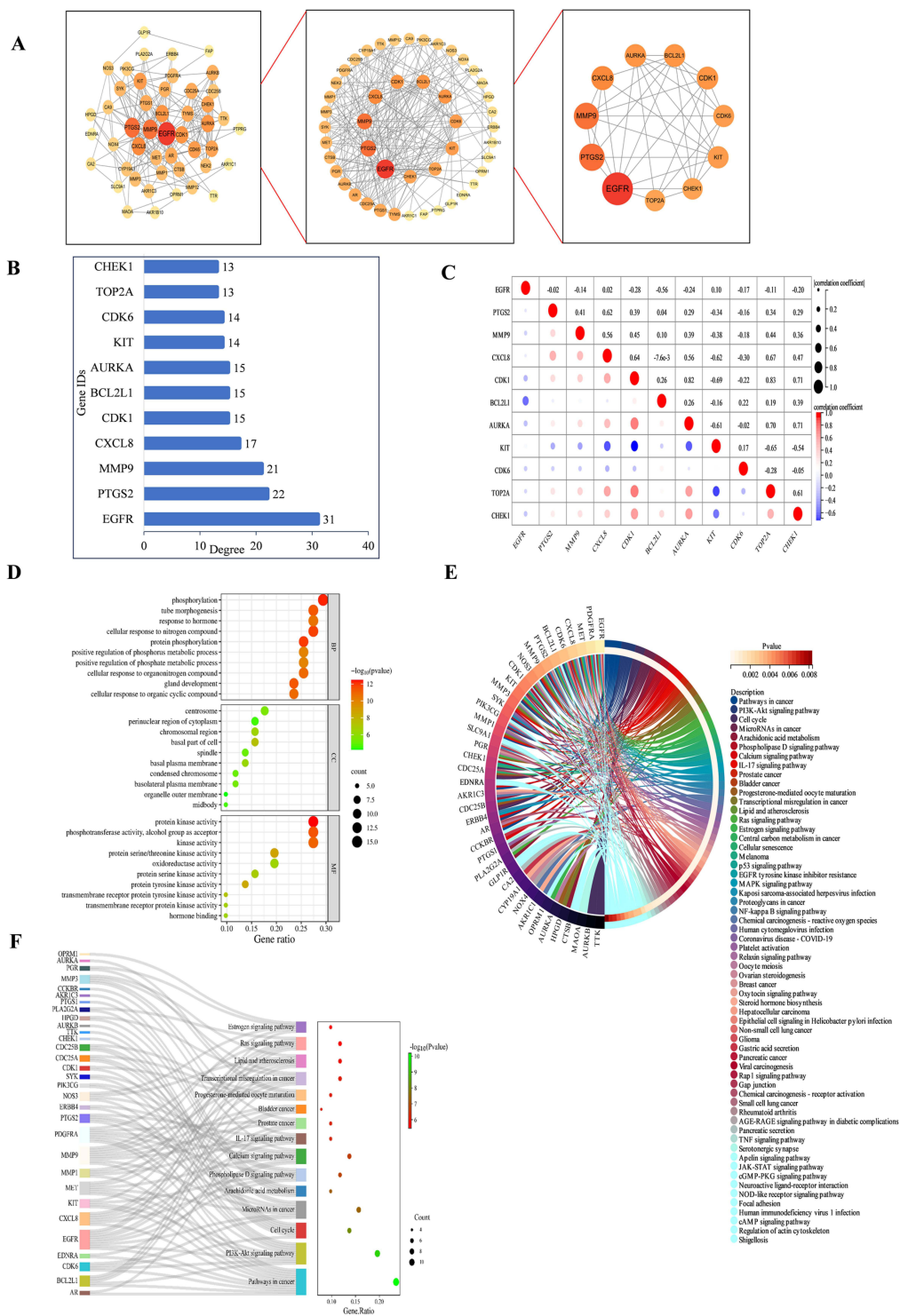


Figure 3 Screening and enrichment analysis of core targets. **(A)** Topology screening process of PPI network, the larger the circle and the redder the color, the more important the target is in the network. **(B)** Degree value of core targets. **(C)** Correlation heatmap of the core targets. Red represents positive correlation, blue represents negative correlation, and darker color indicates stronger correlation. **(D)** GO bubble plots of intersecting targets. The size of the circle represents the number of enriched targets, the bigger the circle, the more targets are enriched. **(E)** KEGG circle diagram of intersecting targets. The outermost left side of the circle represents the pathway; the outermost right side color represents the pathway, and the color of the innermost right side of the circle represents the P-value of the enriched pathway; the lighter the color, the more significant the enriched pathway. **(F)** Ranking of the front KEGG Sankey diagram. The left side represents the intersection target, the middle side represents the pathway, the curve indicates the correlation between the two, and the rightmost bubble graph represents the result of KEGG, the larger the circle, the greener the color, the more significant the enriched pathway.

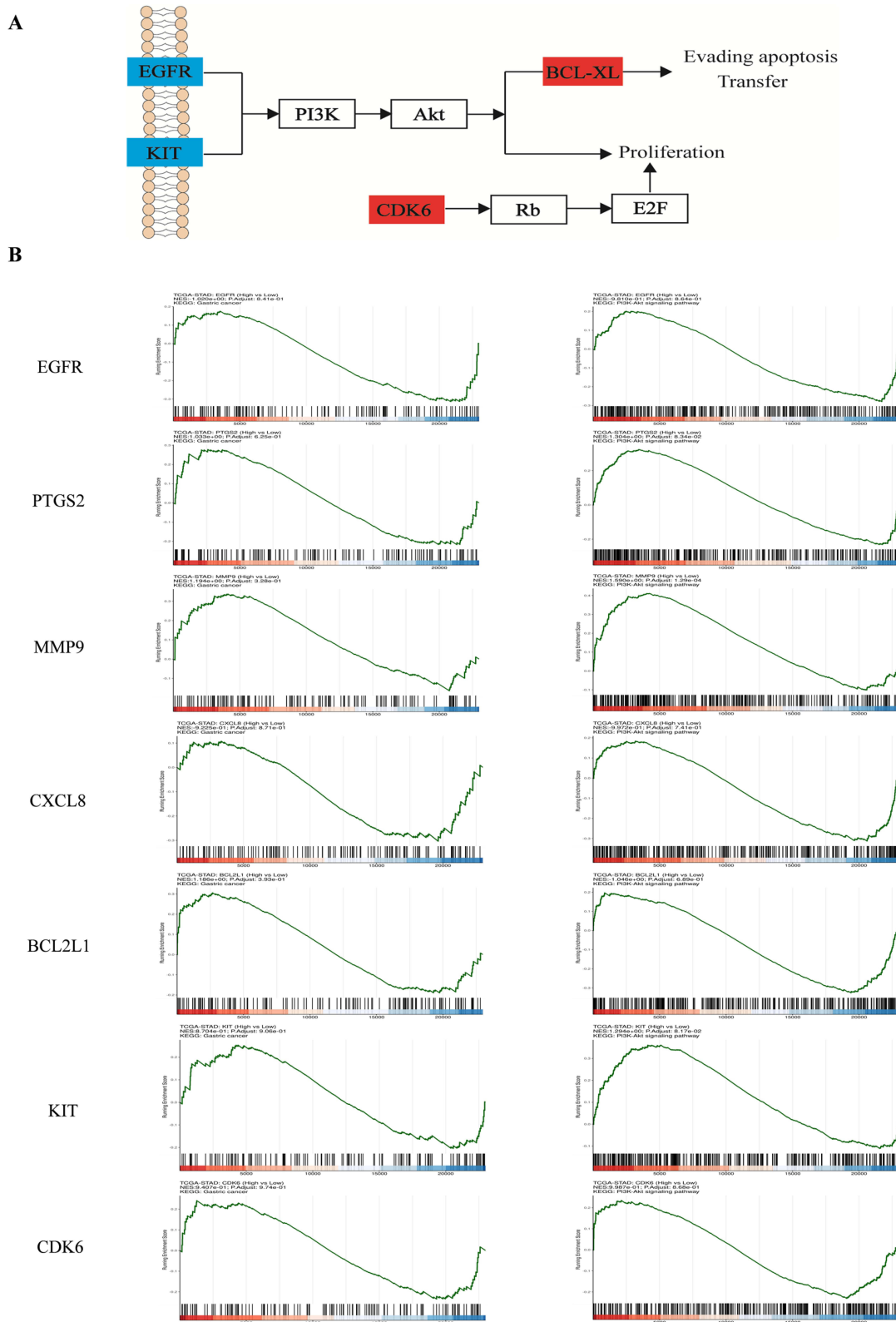


Figure 4 Screening and GSEA analysis of Hub genes. **(A)** Predicting and screening the role of Hub genes in the PI3K-Akt signaling pathway. Red nodes indicate up-regulation related genes and blue nodes indicate down-regulation related genes. **(B)** GSEA analysis graph of Hub genes.

located in this pathway and had a correlation with apoptosis and proliferation, suggesting that ZP-ZR treatment of gastric cancer is primarily related to the PI3K/Akt signaling pathway. In order to compensate for the possible limitation caused by selecting differential genes for the enrichment analysis, GSEA enrichment analysis was performed. The findings indicated that the Hub genes showed positive correlation in both gastric cancer and PI3K/Akt signaling pathway (Figure 4B).

Analysis of Hub Gene Expression and Clinical Correlation

Clinical correlation and prognostic analyses were performed on the seven Hub genes. An analysis was conducted to compare the expression levels of mRNA and protein for seven Hub genes in both normal and gastric cancer tissues. The findings revealed that, relative to normal tissues, gastric cancer tissues exhibited increased mRNA expression levels for PTGS2, MMP9, CXCL8, BCL2L1, and KIT, while a decrease was observed in EGFR mRNA expression (Figure 5A). For Hub gene copy number expression levels, MMP9, CXCL8 and CDK6 hub gene expression were statistically significant (Figure 5B). For Hub gene protein expression levels, EGFR and BCL2L1 were highly expressed in gastric cancer (Figure 5C). The expression levels of Hub genes in gastric cancer subtypes were significantly correlated with patient prognosis. The EBV group exhibited the best prognosis, followed by the MSI and CIN groups, while the GS group had the poorest prognosis.²⁸ The findings indicated elevated expression levels of BCL2L1 and CDK6 in GS, which signaled that the prognosis might be poor (Figure 5D). Among the Hub genes, only the KIT gene shows a significant correlation with the clinical stage of gastric cancer, exhibiting higher expression levels in the middle and advanced stages (Figure 5E). At the same time, because a gene performs its function when it is a protein that performs its function, the expression of the gene at the protein level needs to be detected, and the immunohistochemistry maps of the Hub genes in normal and gastric adenocarcinoma tissues were found (Figure 6A). Additionally, the fluorescence localization maps of the Hub genes in tumor tissues were found (Figure 6B), with green indicating Hub genes, blue indicating nuclei, and red indicating microtubule tissues. The selected Hub genes demonstrated strong clinical correlation, necessitating further verification of their association with patient prognostic survival. The results indicated that EGFR, PTGS2, MMP9, CXCL8, BCL2L1, and KIT, but not CDK6, were correlated with the overall survival (OS) of gastric cancer patients. Specifically, higher expressions of EGFR, BCL2L1, and KIT were associated with shorter survival, while higher expressions of PTGS2, MMP9, and CXCL8 were linked to longer survival (Figure 6C).

Analysis of the Effect of Hub Gene Mutation on Gastric Cancer

Some gene mutations can cause serious tumors. In order to explore whether the Hub genes are mutated to promote the tumor growth, we performed gene mutation-related analyses, including SNV and CNV mutations. Gastric cancer undergoes a series of dynamic gene mutations in tumor cells under the action of various external factors during the process of occurrence and development, and tumorigenesis is characterized by genomic alterations. Therefore, it is essential to analyze the genomic alterations of the seven Hub genes, focusing on SNV and CNV mutations. The seven Hub genes primarily exhibited “Missense-Mutation” at mutation type (Figure 7A; additional genes are detailed in the [Supplementary Figure 1A](#)). The analysis of deleterious mutation frequency in Hub genes across 51 samples revealed that EGFR had the highest mutation frequency, accounting for 41%, followed by MMP9, accounting for 33%, and BCL2L1 and CXCL8 had the lowest mutation frequency, accounting for only 4% (Figure 7B). CNV mutation from genomic rearrangements, including both pure mutation and heterozygous mutation, with pure mutation typically leading to more severe disease. The red and blue colors in the bubble diagram represent amplification and deletion, respectively, and the seven Hub genes have amplification as the main form of mutation, and the larger the bubble, the higher the proportion of mutation. The results indicated a higher proportion of both heterozygous and pure mutations in MMP9 (Figure 7C). For the mutational association of Driver gene with Hub gene, it was analyzed and found that the expression of proto-oncogene could be promoted when EGFR was highly expressed, and the rest of the Hub genes were the same as above (Figure 7D, additional genes are detailed in the [Supplementary Figure 1B](#)). The study found that KIT expression was inversely correlated with MSI in gastric cancer, indicating that higher Hub gene expression corresponded with reduced MSI. Other Hub genes did not show statistically significant correlations (Figure 7E).

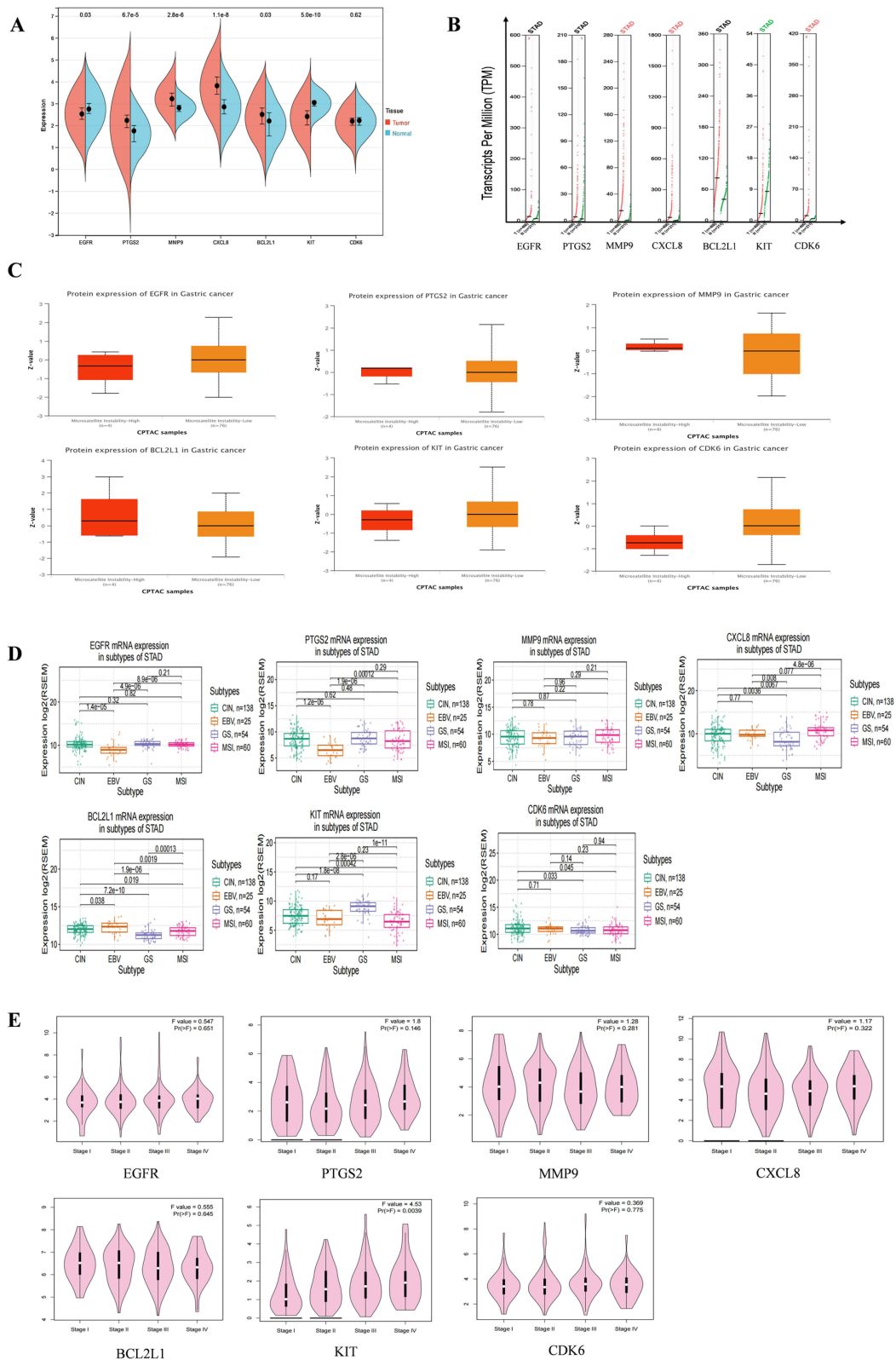


Figure 5 Clinical correlation analysis of Hub gene. **(A)** Expression levels of Hub gene mRNA. Red represents the tumor group and green represents the normal group. **(B)** Expression levels of Hub gene copy number. Red represents the tumor group and green represents the normal group. **(C)** Expression level of Hub gene protein. Red represents the microsatellite instability group and Orange represents the microsatellite stability group. **(D)** Expression levels of Hub gene in gastric cancer subtypes. **(E)** Correlation between Hub gene and clinical stage of gastric cancer.

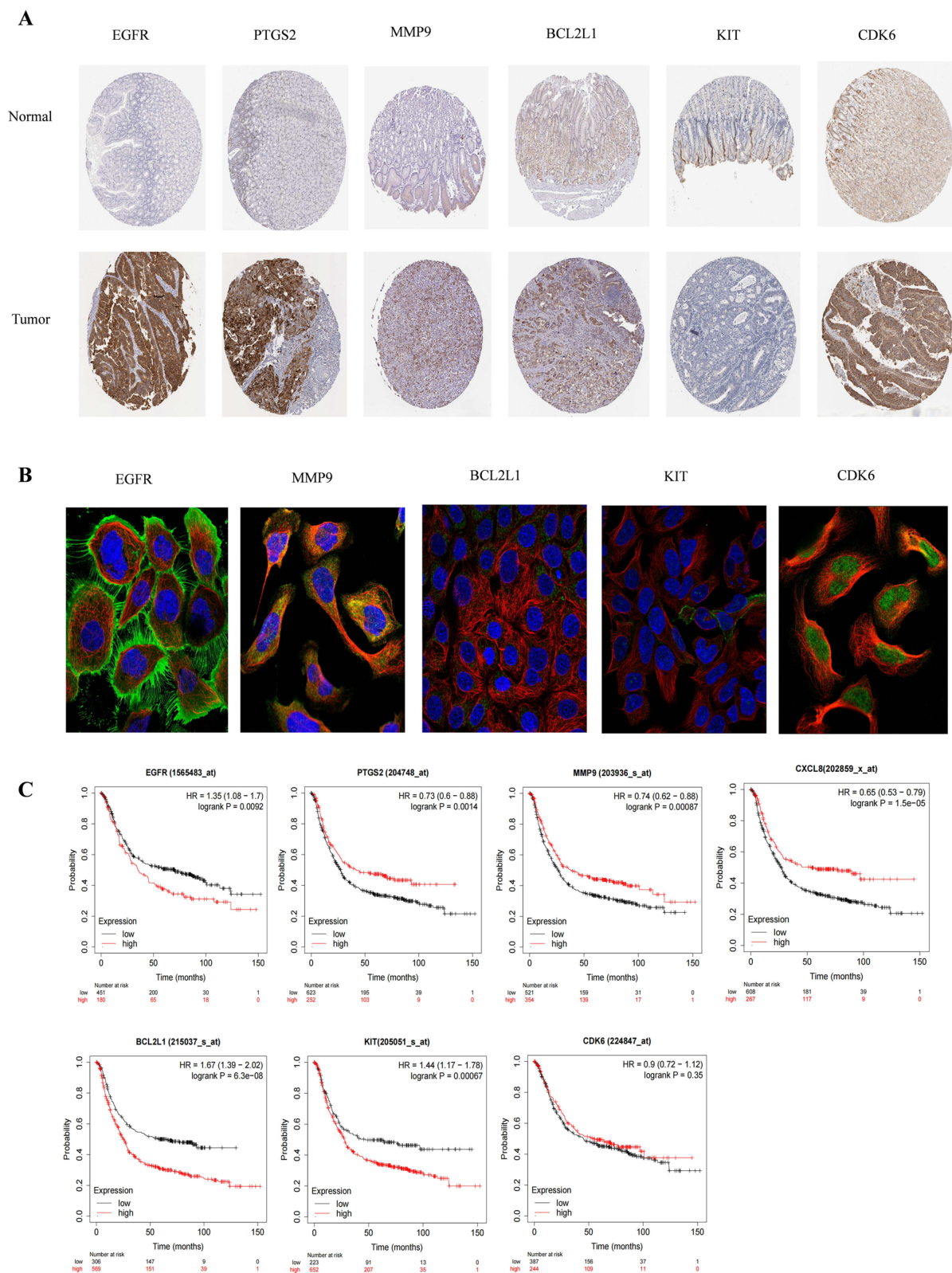


Figure 6 Expression and prognostic analysis of Hub gene. **(A)** Immunohistochemistry of Hub gene in normal gastric tissue and gastric adenocarcinoma tissue. Brown color shows the expression level of Hub gene. **(B)** Fluorescence localization map of Hub gene in tumor tissues. Blue represents nucleus, red represents microtubule organization, and green represents Hub gene. **(C)** Survival curve diagram of Hub gene. The horizontal coordinate represents the survival time.

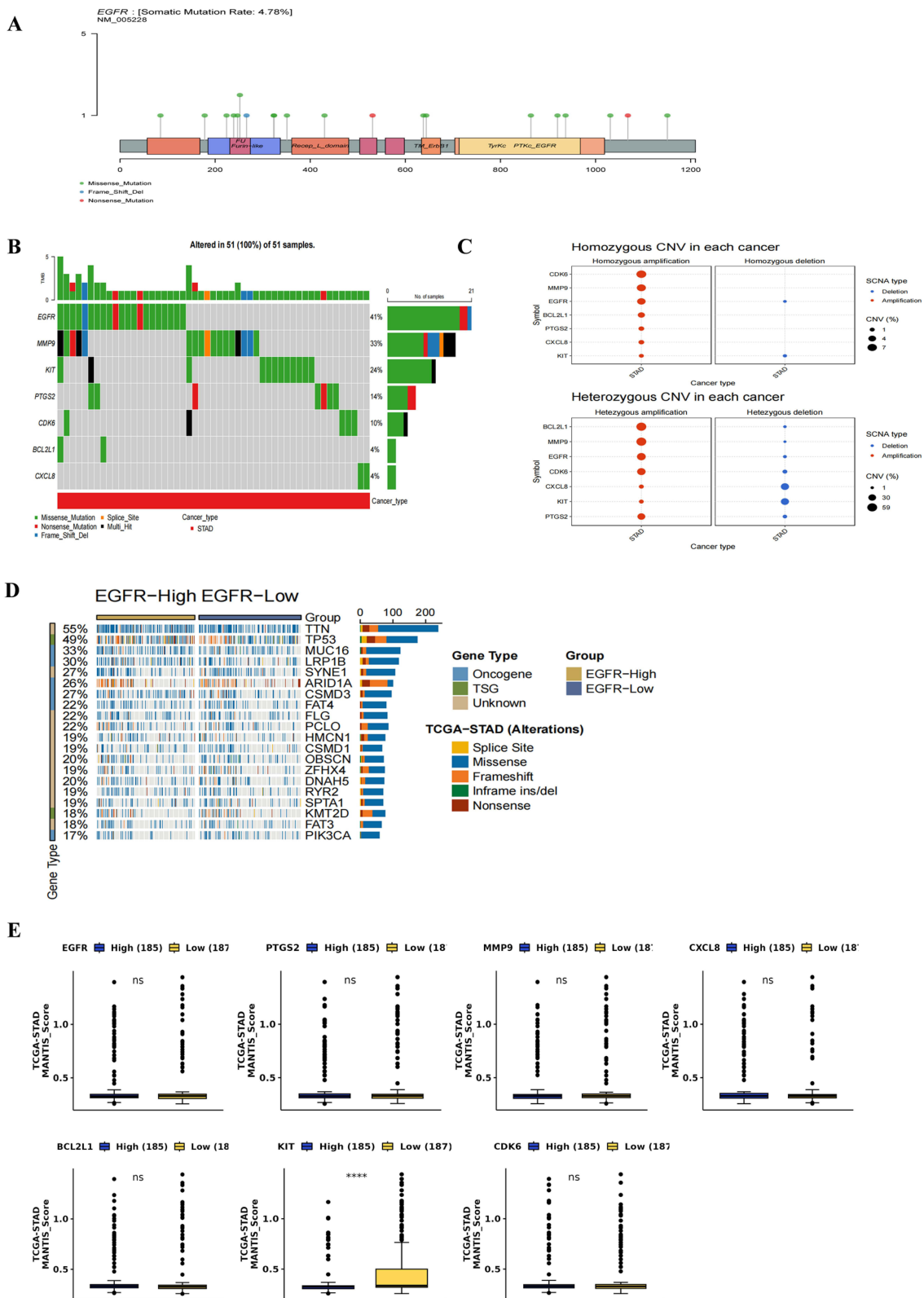


Figure 7 Effect of mutations in the Hub gene on gastric cancer. **(A)** SNV mutation sites and types of EGFR. The circle color represents the mutation type and the line length represents the mutation frequency. **(B)** Waterfall plot of SNV mutation frequency of Hub gene. The upper bar indicates the proportion of Hub gene mutations in the 51 samples. **(C)** Bubble plots of heterozygous and pure heterozygous CNV mutations in the Hub gene. The larger the bubble, the higher the proportion of mutations. **(D)** Mutational associations of Driver genes with the Hub gene. **(E)** Box plot of MSI expression levels of Hub genes. **** and ns represent $P < 0.0001$ and no statistical significance, respectively.

Analysis of Hub Genes in Epigenetic Regulation and Gene Repair

Although, some genes do not significant change from mRNA to protein level, they will show good differences in clinical relevance and may be regulated by methylation, so we perform the methylation analysis. Methylation, a crucial modification of proteins and nucleic acids, regulates the gene expression and silencing. It is a significant focus in epigenetics and encompasses both DNA and protein methylation. Mapping of methylation expression levels of Hub genes showed that the methylation of PTGS2, MMP9, BCL2L1, and KIT in primary cancers all belonged to a low level of expression, while EGFR and CDK6 genes methylation of EGFR and CDK6 genes were all expressed at high levels in primary cancers (Figure 8A). Correlation analysis between Hub gene methylation levels and CTL markers indicated a low correlation for EGFR, PTGS2, MMP9, BCL2L1, KIT, and CDK6, with significant differences observed. CXCL8 showed an extremely low correlation with CTL markers, without significant differences (Figure 8B). The survival curves indicated that hypermethylated subgroups of CXCL8 and BCL2L1 had lower survival rates compared to their hypomethylated counterparts. Additionally, the survival curves for hypermethylated and hypomethylated subgroups of PTGS2, KIT, and CDK6 genes exhibited greater differences (Figure 8C). Gene mutations can promote tumor competition, but there are multiple gene repair systems in vivo that determine genome stability, including the HRR and MMR repair systems, so it is necessary to analyze the correlation between gene mutations and repair systems. The box size represents the correlation magnitude—the larger the box, the stronger the correlation. Results showed that BCL2L1 had the strongest correlation with repair system-related genes, and EGFR had the weakest correlation with it (Figure 8D and E).

Analysis of Hub Genes and Immune Infiltration Relationship

To validate the relevant immune role of gastric cancer genes in cancer, CIBERSORT was used to calculate gastric cancer immune cell infiltration. To examine the correlation between Hub genes and 22 immune cells, the Pearson correlation coefficient was calculated. The visualization results indicated significant differences in nine immune cells in gastric cancer, with the tumor group exhibiting high expression in Correlation and RMSE immune cells (Figure 9A). In the tumor microenvironment, the proportion of immune and stromal cells, significantly impacts prognosis. These non-tumor components are crucial for tumor diagnosis and prognostic evaluation. So we analyzed Hub gene correlation with StromalScore, ImmuneScore, and ESTIMATEScore. The results showed that BCL2L1 and CDK6 genes were negatively correlated with all three scores, and EGFR, PTGS2, MMP9, CXCL8 and KIT genes were positively correlated with all three scores (Figure 9B). The analysis revealed a positive correlation between Hub genes and immune checkpoints, with the exception of a negative correlation observed for the CDK6 gene (Figure 9C). Single-cell sequencing analysis provides insight into the gene expression in single cells. In the gastric cancer GSE167297 dataset, distinct immune cells are color-coded, revealing Hub gene expression across these cells (Figure 9D). PTGS2, MMP9, and CXCL8 were highly expressed in Mono/Macro cells, and BCL2L1 and CDK6 genes were each distributed in the cells. Correlation heatmaps were generated to evaluate the expression values of Hub genes in various immune cells, including macrophages, endothelial cells and CD8⁺ T-cells, larger bubbles and darker colors indicated stronger correlation, and the correlation of MMP9 and KIT with immune cells was higher; the seven Hub genes showed moderate to high correlation with immune cells, especially with monocytes and macrophages (Figure 9E).

Molecular Docking

To evaluate the feasibility of ZP-ZR in treating gastric cancer, seven active components of ZP-ZR were interconnected with the Hub genes EGFR, PTGS2, MMP9, CXCL8, BCL2L1, KIT and CDK6. After docking, the binding activity was evaluated based on binding energy. A smaller binding energy indicated a more stable conformation and a stronger spontaneous binding capacity. Plotting the network diagram of the active ingredient versus the Hub gene (Figure 10A). Making a trilinear plot of the binding energy of the active ingredient versus the Hub gene (Figure 10B). As well as plotting a heatmap to show the effect of the molecular binding activity (Figure 10C). PyMOL software was used to visualize the four binding energies with the lowest docking between Hub gene and active ingredient (Figure 10D), and the results showed that the binding energy of GJ3-CDK6 was the smallest, which was -9.2 kcal/mol.

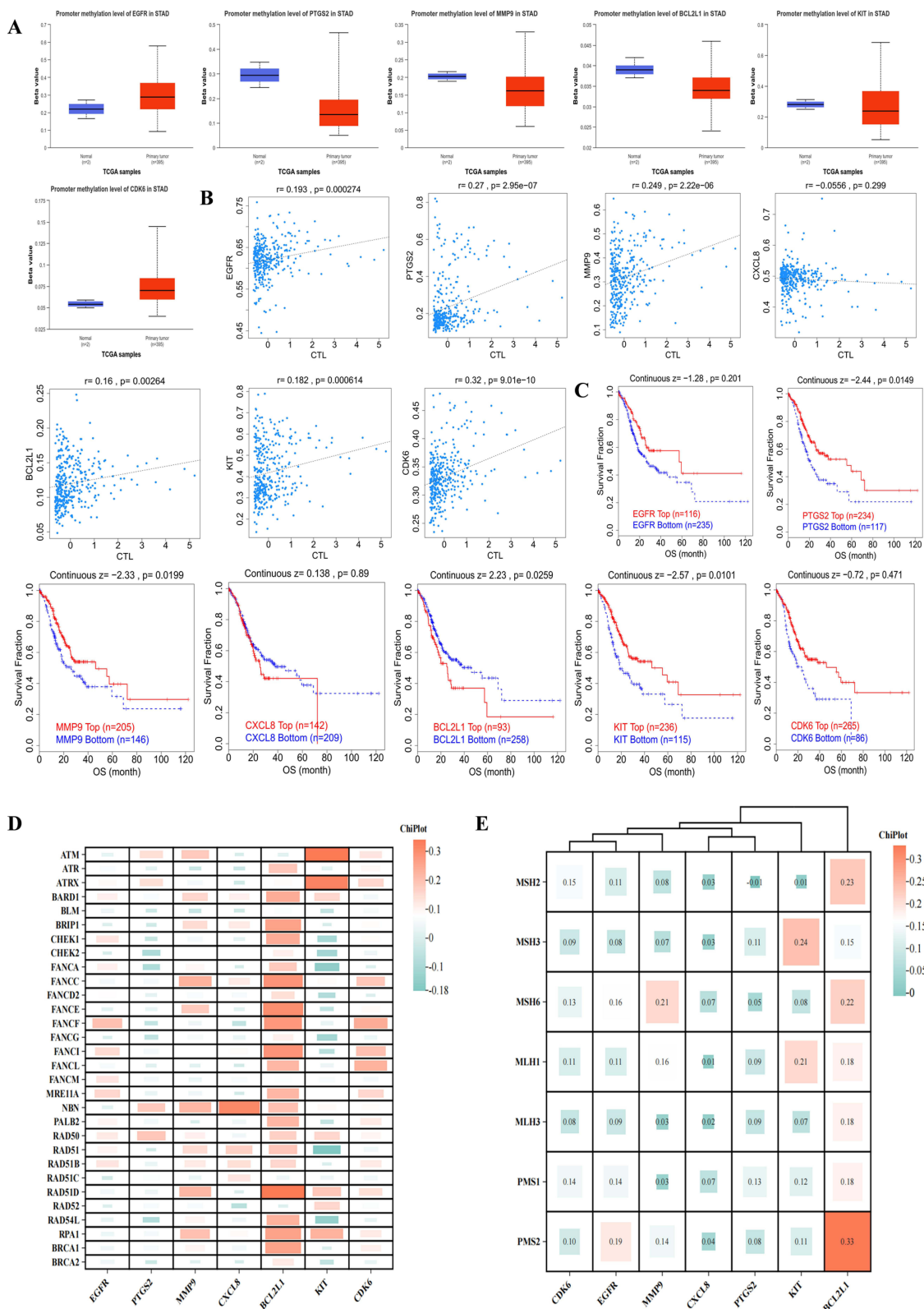


Figure 8 Hub genes are involved in epigenetic regulation and repair of damaged genes. **(A)** Expression level map of Hub gene methylation. Blue and red represent the normal and tumor groups, respectively. **(B)** Correlation between Hub gene methylation levels and CTL markers. **(C)** Survival curves of hypermethylated and hypomethylated subgroups of Hub genes were plotted. **(D and E)** Heatmap of correlation between Hub genes and HRR and MMR repair systems. Red color represents positive correlation and green color represents negative correlation. The size of the box represents the magnitude of the correlation; the larger the box, the stronger the correlation.

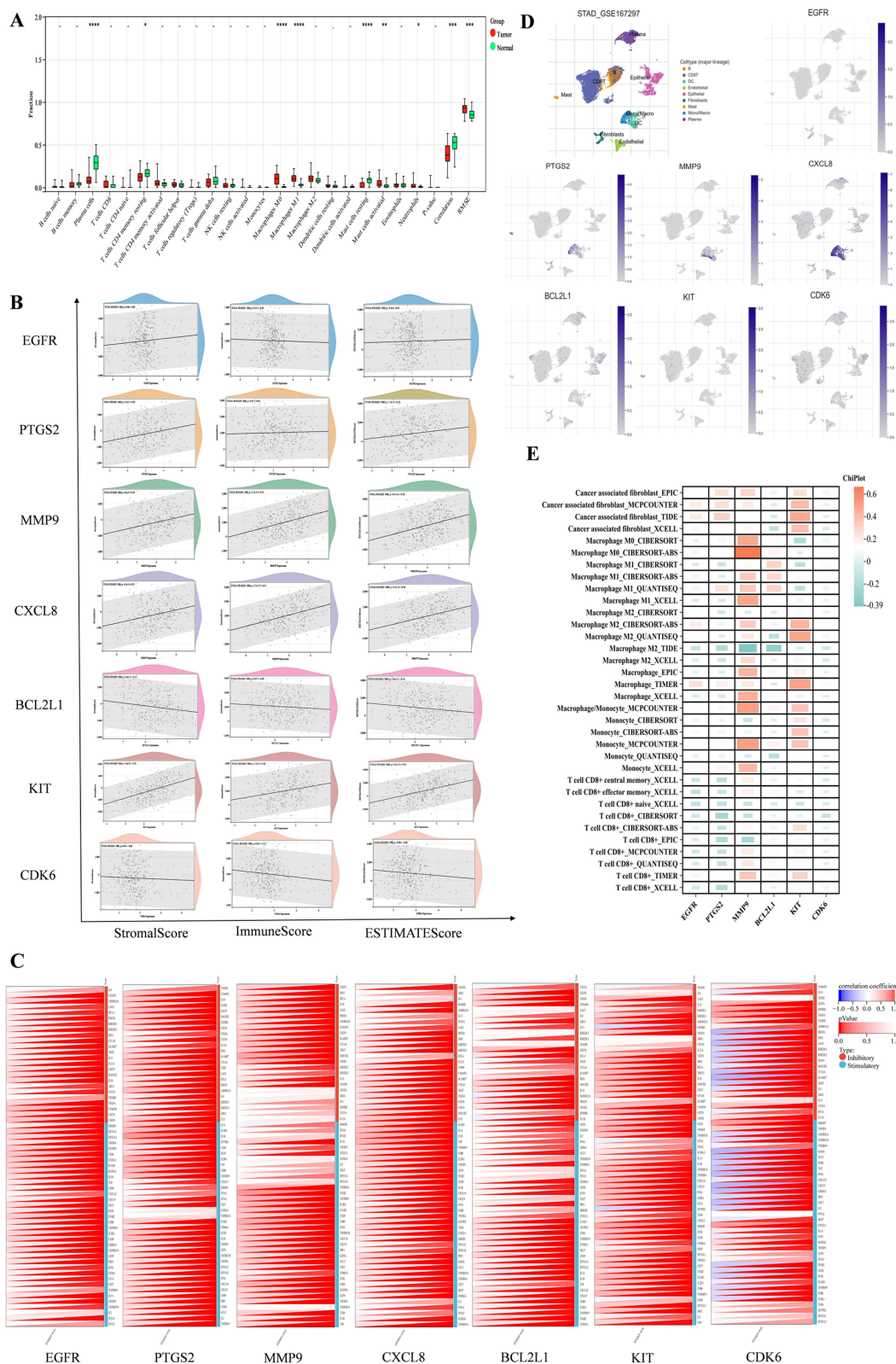


Figure 9 Relationship between Hub genes and immune infiltration. **(A)** Immune cell infiltration in gastric cancer was calculated using CIBERSORT. *, **, ***, **** represent $P < 0.05$, $P < 0.01$, $P < 0.001$, $P < 0.0001$, respectively. **(B)** Scatter plot of StromalScore, ImmuneScore, ESTIMATEScore correlation of Hub gene **(C)** Heatmap of correlation between Hub genes and immune checkpoints. Blue color represents negative correlation and red color represents positive correlation. **(D)** Single-cell sequencing (top) and single-cell annotation map (bottom) of Hub genes. Different colors represent different sets of cells. **(E)** Hub gene correlates with macrophage, endothelial cell, tumor-associated fibroblast, and CD8+ T cell infiltration. Green represents negative correlation, red represents positive correlation, and larger box and darker colors represent stronger correlation.

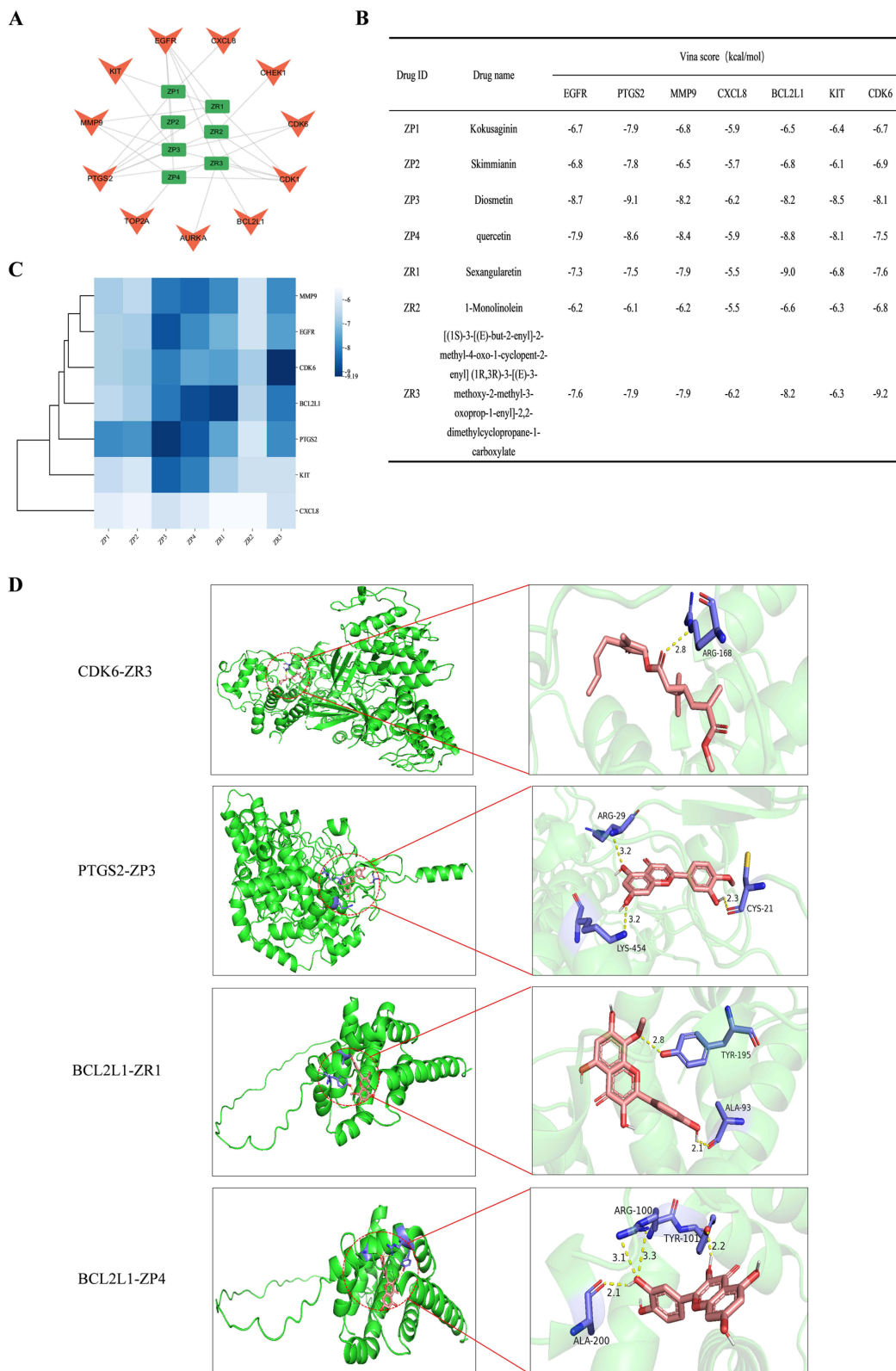


Figure 10 Molecular docking of Hub genes with core active ingredients (A) Screening of core active ingredients exerting anti-gastric cancer therapeutic effects, with red triangles representing the targets and green rectangles representing the abbreviated names of the active ingredients. (B and C) Molecular docking binding energy of Hub genes and core active ingredients. (D) Visual demonstration of partial molecular docking.

Results of Cell Experiments

Effect of ZP-ZR on the Viability of Gastric Cancer Cells

Gastric cancer cells were treated with varying concentrations of ZP-ZR to assess its impact on cell viability. The results of the CCK8 assay demonstrated that ZP-ZR markedly decreased the viability of both AGS and HGC-27 cells, with higher concentrations of ZP-ZR correlating with decreased cell viability (Figure 11A and B). Figure 11D summarizes the low, medium and high concentrations of AGS and HGC-27 cells at 24 hours of drug intervention: AGS cells at 16, 18, and 20 mg/mL, and HGC-27 cells at 8, 12, and 16 mg/mL. GES-1 cells were treated with ZP-ZR at concentrations ranging from 0 to 20 mg/mL to assess toxicity. At 18 mg/mL, cell viability remained above 80% ($P < 0.05$), indicating that ZP-ZR effectively inhibited gastric cancer cell viability after 24 hours of treatment while exhibiting minimal toxicity to normal cells. Therefore, 24h was chosen as the time of drug intervention (Figure 11C).

Effect of ZP-ZR on Cell Apoptosis

Upon 24 hours of treatment, the gastric cancer cells exhibited an apoptosis rate that was directly proportional to the increased concentrations of ZP-ZR. After 24 hours of ZP-ZR intervention on AGS cells, apoptosis rates for low, medium, and high concentrations were $16.6 \pm 0.1\%$, $23.28 \pm 0.27\%$, and $28.45 \pm 0.57\%$, respectively, all of which were elevated compared to the control group's rate of $5.41 \pm 0.13\%$ (Figure 11E and F). In HGC-27 cells, apoptosis rates were $9.88 \pm 0.46\%$, $17.99 \pm 0.39\%$, and $39.46 \pm 0.32\%$, respectively, all exceeding the control group's rate of $3.88 \pm 0.35\%$ (Figure 11G and H).

Effects of ZP-ZR on Cell Cycle Blockade in Gastric Cancer

Our observations revealed that both AGS and HGC-27 cells underwent cell cycle arrest at the G0/G1 phase. After 24 hours of ZP-ZR treatment, the proportion of blocked cells in the G0/G1 phase increased significantly, with percentages of $44.06 \pm 1.21\%$, $49.93 \pm 0.21\%$, $55.2 \pm 1.59\%$, and $62.33 \pm 2.55\%$ in the AGS cell control, low, medium, and high dose groups, respectively (Figure 11I and J). In HGC-27 it was $35.36 \pm 0.81\%$, $40.17 \pm 0.9\%$, $42.63 \pm 0.56\%$ and $45.88 \pm 0.73\%$, respectively (Figure 11K and L). Cell cycle proteins regulate progression by binding to cyclin-dependent kinase (CDK), with CDK 6 primarily involved in G0/G1 phase regulation. Western blot analysis revealed a decrease in CDK 6 levels after HGC-27 exposure to ZP-ZR for 24 hours, consistent with cell cycle findings.

Effect of ZP-ZR on the Formation of Cellular Clones

Cell counts were analyzed using ImageJ software, and the results indicated that AGS cells exhibited reduced colony formation compared to the control across low, medium, and high concentrations, with a progressive decline as the concentration increased (Figure 11M and N). Similarly, HGC-27 cells showed decreased colony formation at low, medium, and high concentrations, with further reductions observed as concentration increased (Figure 11O and P).

ZP-ZR Inhibits Cellular Horizontal Migration Ability

The effect of ZP-ZR on the horizontal migration capacity of cells was determined to use a wound healing experiment. Separate interventions were performed for 24h. The number of cells covering the scratched area increased over time compared to the 0-hour mark. ZP-ZR significantly reduced the migration rate of AGS cells in a dose-dependent manner compared to the control (Figure 12A and B). Low, medium, and high concentrations of ZP-ZR significantly reduced the migration rate of HGC-27 cells compared to the control (Figure 12C and D). The inhibitory effect of ZP-ZR on cell migration was positively correlated with its concentration, with higher concentrations leading to a greater reduction in migratory ability.

ZP-ZR Inhibits Vertical Cell Migration and Invasion

Cell invasion is a form of cell migration and the two are inextricably linked. Cancer cells break through the basement membrane, endocytosis into blood vessels and lymphatic vessels, and invade from one area to another. Cell migration and invasion assays, as a commonly used biomedical experiment aimed at assessing the invasive and migratory capacity of cells, in particular the simulation and observation of cell behavior in a physiological environment mimicking the *in vivo* environment. They are generally most commonly used in studies of tumor malignancy phenotypes.²⁹ Transwell migration assay was performed to detect the effect of ZP-ZR on the vertical migration ability of AGS and HGC-27 cells

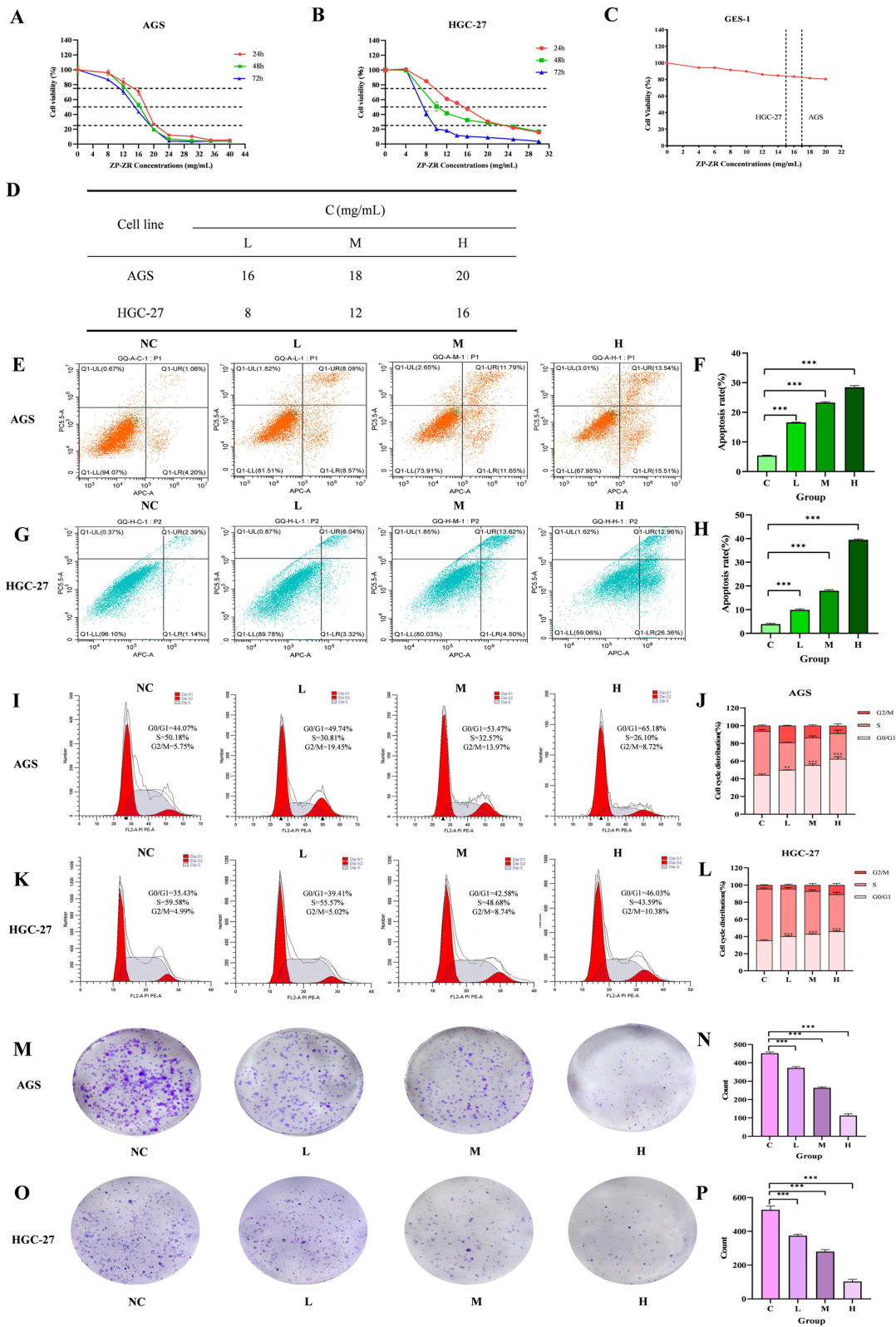


Figure 11 ZP-ZR suppressed cell viability, induced apoptosis and blocked the cell cycle in gastric cancer cells (**A** and **B**) AGS and HGC-27 cells were treated with different concentrations of ZP-ZR for 24 h, 36 h and 48 h. (**C**) The GES-1 cell were treated with different concentrations of ZP-ZR for 24 h. (**D**) IC50 values for 24, 36, and 48 h of AGS and HGC-27 cells. (**E-H**) The effect of different concentrations of ZP-ZR on the apoptosis rate in AGS and HGC-27 cells. (**I-L**) Effects of ZP-ZR on the cell cycle of AGS and HGC-27. (**M-P**) Observed the effects of different concentrations in AGS and HGC-27 cells under the mi-croscope. All datas were expressed as mean \pm SD. *** $P < 0.001$.

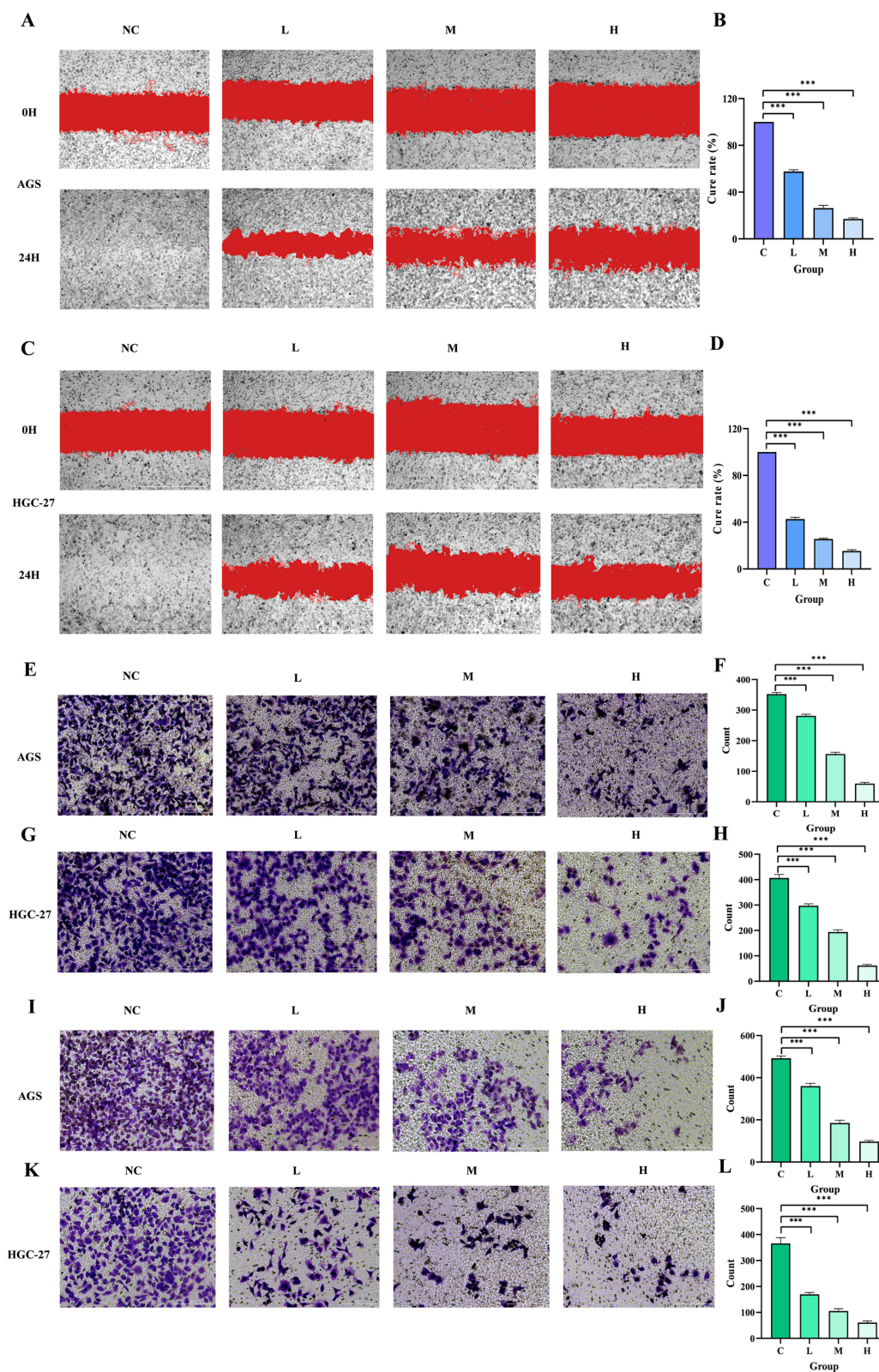


Figure 12 Effects of ZP-ZR on migration of AGS and HGC-27 cells in gastric cancer. (A–D) Effect of ZP-ZR on horizontal migration of AGS and HGC-27 cells after 24h intervention. (E–H) Effect of ZP-ZR on vertical migration of AGS and HGC-27 cells after 24h intervention. (I–L) Effect of ZP-ZR on the invasion ability of AGS and HGC-27 cells after 24h intervention. All datas were expressed as mean \pm SD. *** $P < 0.001$.

by observing the changes in the number of cells in the Transwell chambers. Separate interventions were performed for 24h using low, medium and high concentrations of the drug for different cells. The Transwell migration assay demonstrated that ZP-ZR significantly reduced the vertical migration of AGS cells across the membranes at other groups, compared to the control group (Figure 12E and F). Low, medium and high concentrations of ZP-ZR significantly reduced the number of HGC-27 cells penetrating the membrane compared to the control (Figure 12G and H). The Transwell invasion assays further revealed that other groups, markedly reduced the number of AGS cells penetrating the membrane compared to the control group, indicating a concentration-dependent decrease in invasive ability (Figure 12I and J). Compared to the control group, other groups reduced the invasion ability of HGC-27 cells in a concentration-dependent manner (Figure 12K and L).

Effect of ZP-ZR on Cellular mRNA Expression

The qRT-PCR experiment is to quantify the unknown template by the standard curve of fluorescence signal. Network pharmacology analysis indicates that ZP-ZR can modulate the mRNA levels of seven Hub genes, potentially key targets against gastric cancer. Therefore, qRT-PCR was employed to assess the expression of these Hub genes. ZP-ZR (12 mg/mL) significantly decreased the expression of EGFR, PTGS2, MMP9, CXCL8, BCL2L1, KIT, and CDK6 in HGC-27 cells after 24 hours, compared to the control group (Figure 13A). The qRT-PCR results were analyzed using *t*-test.

Effects of ZP-ZR on PI3K/Akt Signaling Pathway

Western blot assay is a method for specific detection of target proteins. Therefore, Western blot assay was employed to examine the impact of ZP-ZR on PI3K/Akt signaling pathway protein expression. Following 24 hours of ZP-ZR treatment, HGC-27 cells exhibited significant down-regulation of EGFR, KIT, BCL2L1, and CDK6 expressions compared to the control group. The expression of Akt and PI3K in the ZP-ZR intervention group had no significant change trend. In contrast, the expressions of both p-Akt and p-PI3K were significantly down-regulated (Figure 13B and C). Therefore, ZP-ZR may inhibit the activation of the PI3K/Akt signaling pathway.

Discussion

In this study, we utilized network pharmacology and molecular docking to screen the active ingredients as well as the core targets of ZP-ZR to predict the possible action relationship between ZP-ZR and gastric cancer for effective alternative or adjuvant therapy. The study identified 7 active ingredients, 51 intersecting targets, and 60 related pathways of ZP-ZR associated with gastric cancer. Potential Hub genes such as EGFR, PTGS2, MMP9, CXCL8, AURKA, BCL2L1, and CDK1 were obtained through PPI network interactions. Through the analysis of pathway-enriched targets in cancer, seven Hub genes—EGFR, PTGS2, MMP9, CXCL8, BCL2L1, CDK6, and KIT—were identified, which collectively act as antitumor agents to modulate the mechanism of action in gastric cancer. GO and KEGG Enrichment analysis showed that the Hub gene exerted the most significant effects against gastric cancer primarily through involvement in the PI3K/Akt signaling pathway, which in turn extends to the cell cycle pathway. Upon validating the Hub genes within the GEPIA, GSCA, and UALCAN databases, it was evident that a majority of Hub genes exhibited elevated expression levels in gastric cancer tissues relative to normal ones, accompanied by enhanced clinical pertinence and prognostic implications. Through molecular docking, it was confirmed that the Hub genes had strong interaction with the active ingredients. Finally, we performed in vitro cellular experiments to verify the effect of ZP-ZR on gastric cancer. CCK-8 results indicated that ZP-ZR reduced gastric cancer cell viability while exhibiting lower toxicity to normal cells. ZP-ZR inhibited gastric cancer cell proliferation by blocking the G0/G1 phase of the cell cycle and inducing apoptosis. Wound healing experiment and Transwell assay demonstrated that ZP-ZR treatment significantly inhibited the migration and invasion of gastric cancer cells. The mechanisms were explored by qRT-PCR and Western blot at gene and protein levels, respectively. The mRNA levels of EGFR, PTGS2, MMP9, CXCL8, BCL2L1, CDK6, and KIT were significantly reduced after 24 hours of ZP-ZR intervention. We analyzed the expression levels of key proteins in the PI3K/Akt pathway identified by KEGG. It was confirmed by Western blot that ZP-ZR reduced the protein expression of p-PI3K, p-Akt, EGFR, KIT, BCL2L1 and CDK6. Therefore, we postulated that ZP-ZR might elicit its effects by modulating the suppression of gastric cancer cell proliferation as well as metastasis via the PI3K/Akt signaling pathway, arresting the cell

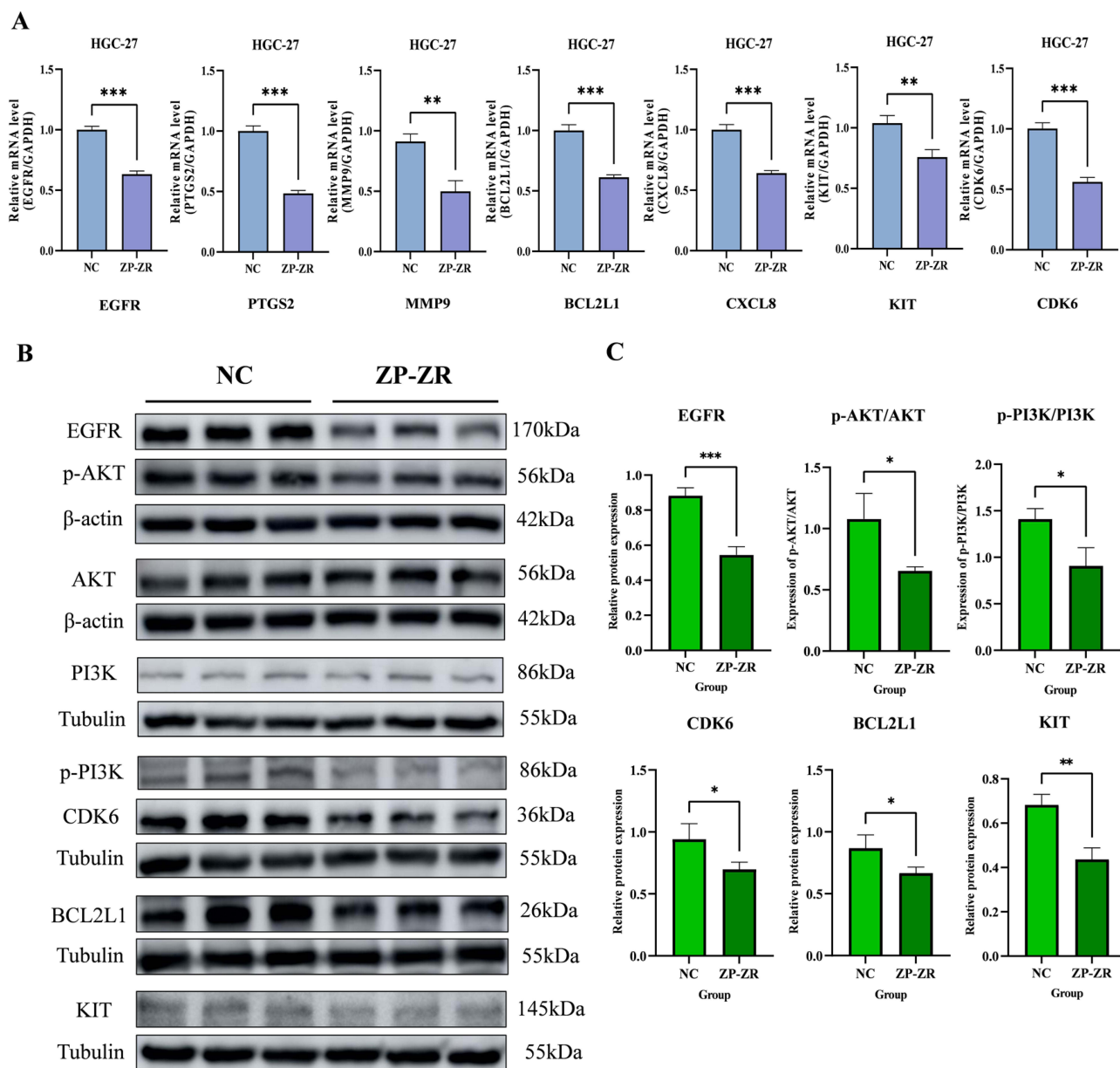


Figure 13 ZP-ZR regulated hub genes and PI3K/Akt signaling pathway. **(A)** mRNA level of 7 hub genes in AGS and HGC-27 cells treated with ZP-ZR for 24 h. **(B and C)** Level of key proteins in PI3K/Akt signaling pathway after ZP-ZR treatment of AGS and HGC-27 cells for 24 h. All data were expressed as mean \pm SD. * $P < 0.05$, ** $P < 0.01$, *** $P < 0.001$.

cycle, stimulating apoptosis, and impeding cell migration and invasive capacity. A mechanistic model illustrating the potential mechanism of ZP-ZR in gastric cancer was proposed based on these results, as shown in Figure 14.

Network pharmacological analysis predicted key active ingredients in ZP-ZR for treating gastric cancer, including Kokusaginin, Skimmianin, Diosmetin, Quercetin, Sexangularetin, and 1-Monolinolein. Kokusaginin, a natural furan quinoline alkaloid, has been shown in the literature as one of the biologically active natural products isolated from the aerial parts of the plant. Notably, it has significant anti-inflammatory, antioxidant and/or antiproliferative properties.³⁰ Meanwhile related literature assessed the cytotoxicity of a large number of isolated metabolites of cytotoxic benzophenanthridines and furanquinoline alkaloids from *Zanthoxylum armatum*, which included kokusaginin, against a range of multidrug-resistant cancer cell lines, with kokusaginin displaying selective cytotoxicity.³¹ Recent research indicates that Kokusaginin exhibits cytotoxic effects on various human cancer cell lines, including HeLa, A431, MCF-7, and A2780, and induces cell cycle arrest in a concentration-dependent manner.³² However, the mechanism of action of this active

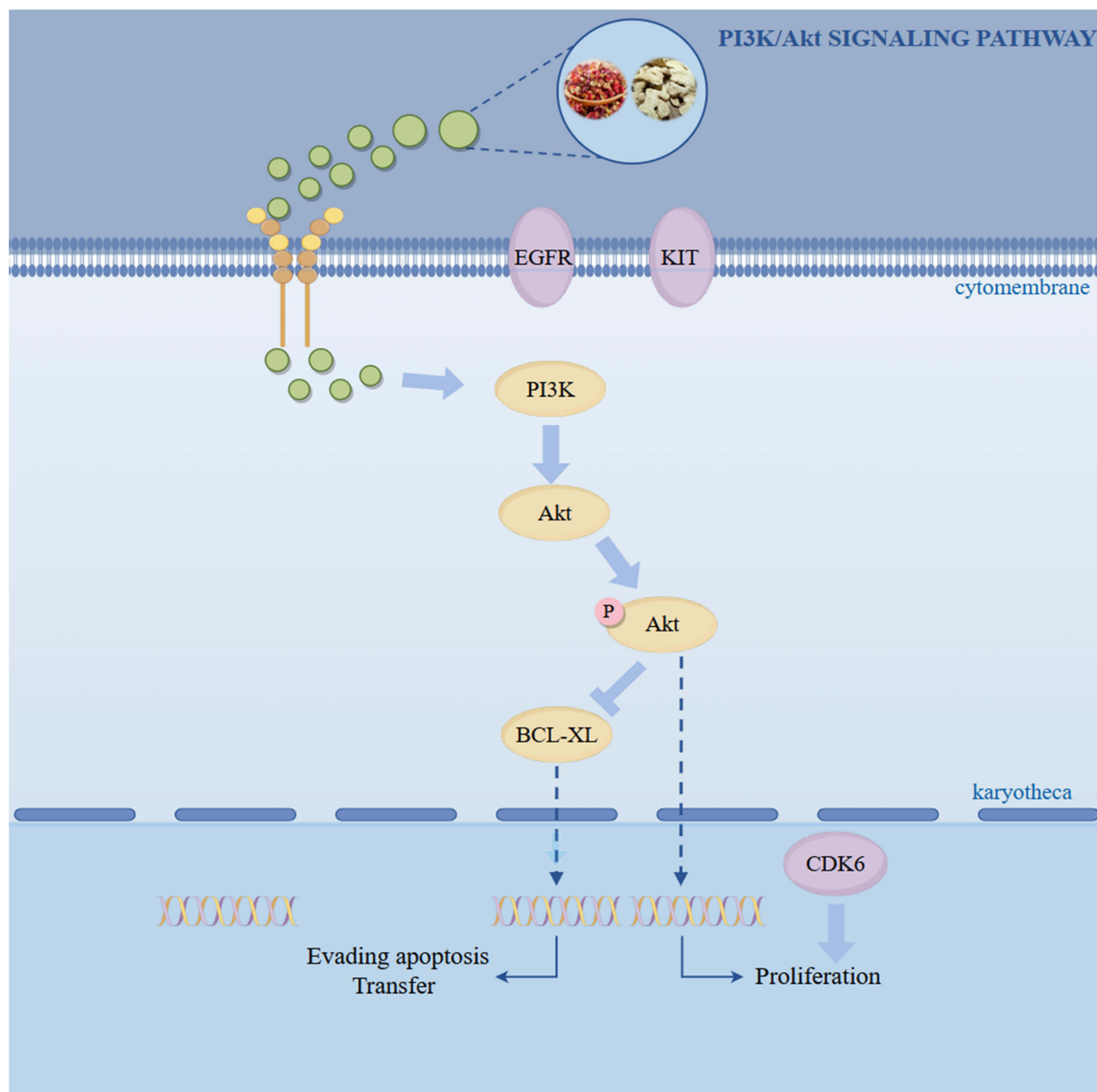


Figure 14 Mechanism diagram of ZP and ZR anti-gastric cancer.

ingredient on gastric cancer is less studied and we need to explore it further. Skimmianie is a naturally occurring furanquinoline alkaloid derived from rutaceous family plants. Research indicates that Skimmianie may protect against the liver injury by regulating inflammation, apoptosis, and oxidative stress through the PI3K/Akt signaling pathway.³³ In addition, Skimmianie inhibited human esophageal squamous cell carcinoma proliferation and migration by blocking ERK1/2 activation, regulating epithelial-mesenchymal transition (EMT) and significantly reducing xenograft tumor growth in nude mice.³⁴ Therefore, Skimmianie is an active ingredient in anti-tumor, but there are fewer studies related to gastric cancer. Diosmetin is a natural flavonoid constituent with anti-inflammatory,³⁵ antimicrobial,³⁶ and antioxidant properties,³⁷ and has shown promising results in anti-tumor. Diosmetin inhibits gastric cancer cell growth and invasion by interfering with M2 macrophage polarization through the TRAF2/NF- κ B signaling pathway.³⁸ In colorectal cancer HCT-116 cells, Diosmetin can promote apoptosis by inhibiting NF- κ B translocation and disrupting mitosis.³⁹ Quercetin,

a natural flavonoid found in fruits and vegetables, exhibits cardiovascular protection, anti-inflammatory, and anti-tumor activities. Relevant literature shows that Quercetin disrupts uPA/uPAR function by regulating NF- κ B, PKC- δ , ERK1/2 and AMPK α , and has anti-metastatic function on gastric cancer cells.⁴⁰ Sexangularetin, a flavonoid identified by Wanli Ji et al through network pharmacology as a key active ingredient from the active ingredient-target network of *Semixia laxative* heart soup. The study demonstrated that *Semixia laxative* heart soup mitigated the severity of ulcerative colitis by inhibiting the Akt/MAPK signaling pathway.⁴¹ 1-Monolinolein, a type of 1-Monoacylglycerol, has been identified as an active component in *Zingiberis Rhizoma* for colon cancer treatment. 1-Monolinolein plays a pivotal role in the mechanism of colon cancer prevention by *Zingiberis Rhizoma* through the tumor pathway and PI3K/Akt signaling pathway.⁴² The above ZP-ZR active ingredients significantly inhibit growth and induce apoptosis in various solid tumors through multiple regulatory mechanisms. However, the mechanisms regulated by ZP-ZR active ingredients in gastric cancer remain underexplored and uncertain, necessitating further investigation.

This study analyzes PPI network interactions and performs GO and KEGG functional enrichment. Meanwhile, according to the relevant literature, the Hub gene of the direct interaction between ZP-ZR is crucial in the treatment of gastric cancer and the elucidation of its mechanism of action. EGFR, part of the ERBB family of receptor tyrosine kinases, undergoes autophosphorylation and activates downstream signaling upon binding to its ligands (eg, EGF and TGF- α), promoting cell proliferation and metastasis.⁴³ Inhibiting PTGS2 (Cyclooxygenase (COX)-2) expression can suppress tumor cell proliferation and induce apoptosis.⁴⁴ CXCL8 (Interleukin-8) serves as a crucial autocrine regulator in the cancer microenvironment and acts as a pro-angiogenic mediator, promoting angiogenesis in various cancers.⁴⁵ This indicates that IL-8 is pivotal in gastric carcinogenesis and metastasis. The BCL2L1 (Bcl-XL) gene encodes a protein from the Bcl-2 family that functions as either anti- or pro-apoptotic regulators in various cellular activities. The encoded protein localizes to the mitochondrial membranes and regulates programmed cell death during development and tissue homeostasis. Research indicates that modulating BCL2L1 gene expression, increasing caspase-3 activity, and inducing apoptosis can inhibit the proliferation of SGC-7901 cells.⁴⁶ MMP9 expression within the MMP family is linked to increased angiogenesis in tumor cells and is crucial for gastric cancer invasion and metastasis, thereby promoting tumor progression.⁴⁷ KIT is one of the key members of the tyrosine kinase receptor protein family, and literature shows that the majority of gastrointestinal mesenchymal stromal tumors (GIST) have mutations in the KIT gene, which leads to uncontrolled KIT protein-stimulated sustained proliferation and anti-apoptotic signaling in tumor cells.⁴⁸ Cell cycle protein-dependent kinase (CDK) 6 cell cycle regulator, which can lead to cell cycle disorders, is closely related to cancer development. Literature indicates its involvement in gastric cancer progression by modulating CDK6 expression and thus by influencing the proliferation and migration of gastric cancer cells.⁴⁹ The above results have confirmed that EGFR, PTGS2, MMP9, CXCL8, BCL2L1, CDK6 and KIT are closely associated with the development of gastric cancer. In order to further observe the correlation between these seven Hub genes and gastric cancer, through the process of GSEA analysis, clinical relevance analysis, molecular docking validation and cellular experiments has been confirmed that the regulatory role of these Hub genes in gastric cancer.

We utilized pathway enrichment analysis and revealed that ZP-ZR is linked to the PI3K/Akt signaling pathway and extends to the cell cycle pathway. The PI3K/Akt pathway, a well-known anti-apoptotic and survival signaling mechanism, has recently been linked to tumor development. This pathway promotes tumor proliferation, metastasis, and invasion by activating various cytokines, phosphorylating downstream CREB transcription factors, and facilitating their nuclear entry to regulate the cell cycle and inhibit apoptosis and metastasis-related gene expression.²² Relevant literature indicates that ginsenoside CK inhibits the anti-apoptotic protein Bcl-2 and the PI3K/AKT/NF- κ B pathway, while promoting pro-apoptotic proteins Bax and Caspase 3, thereby inducing apoptosis and inhibiting the proliferation of gastric cancer cells.⁵⁰ Meanwhile, cell cycle control is becoming one of the major research areas in the field of cancer prevention. Cell cycle disorders due to unbalanced secretion of cell cycle elements are one of the characteristics of tumor cells. CDK and cell cycle proteins are closely associated with tissue development and carcinogenesis by regulating the cell cycle. Cam et al found that CDK6 protein expression was dysregulated in tumor cells and that up-regulated expression of CDK6 proteins phased G1 longer in cells and promoted proliferation. Increased cell proliferation or decreased apoptosis is the beginning of carcinogenesis.⁵¹

In conclusion, network pharmacology and in vitro cellular experiments have demonstrated that ZP-ZR may inhibit gastric cancer cell proliferation, block the cell cycle, induce apoptosis, and reduce cell migration and invasion through the PI3K/Akt signaling pathway. Additionally, ZP-ZR appears to be involved in immune regulation mechanisms, offering a theoretical basis and scientific evidence for future tumor treatments using related TCM pairings. However, due to time constraints, we only performed cellular experiments, which have limitations. We dissolved ZP-ZR particles in a water bath to directly intervene in AGS and HGC-27 cells. However, if administered orally, some of the components of ZP-ZR that play an active role in anticancer cells may not be able to reach the target organ to exert anticancer effects. Therefore, we plan to carry out in vivo animal experiments in nude mice with tumorigenicity, and conduct histological analysis of the active components that enter the blood and tissues to explore the active components that finally reaches the target organs, to further explore the anti-gastric cancer effects of ZP-ZR. Meanwhile, the causal relationship between upstream and downstream proteins in the PI3K/Akt signaling pathway was confirmed through Co-IP and gene silencing experiments. Transcription factor regulation was assessed using dual luciferase and CHIP assays. The specific anti-gastric cancer mechanism of ZP-ZR was investigated to facilitate its application in gastric cancer treatment.

Abbreviations

GC, gastric cancer; ZP-ZR, Zanthoxyli Pericarpium-Zingiberis Rhizoma; TCM, traditional Chinese medicine; GO, Gene Ontology; KEGG, Kyoto Encyclopedia of Genes and Genomes; OB, oral bioavailability; DL, druglikeness; PPI, protein-protein interaction; BP, biological process; MF, molecular function; CC, cellular composition; qRT-PCR, quantitative real time polymerase chain reaction; StromalScore, stroma in the tumor tissue; ImmuneScore, immune cell infiltration in tumor tissue; ESTIMATEScore, tumor purity; EMT, epithelial-mesenchymal transition; GIST, gastrointestinal mesenchymal stromal tumors.

Statement of Ethics

This study was exempted from approval in accordance with Article 32, paragraphs 1 and 2 of the Measures for Ethical Review of Life Science and Medical Research Involving Human Beings issued on February 18, 2023 in China. This research uses human information data or biological samples to conduct life science and medical research that does not cause harm to human beings or involve sensitive personal information or commercial interests; this research is conducted using legally obtained public data or data generated by observation without interfering with public behavior; and this research is conducted using anonymized information data.

Acknowledgments

The authors acknowledge any support given which is not covered by the author contribution or funding sections.

Funding

Ningxia Key Research and Development Program (No.2023BEG02015); Ningxia Natural Science Foundation (2023AAC03222); Talent Development Projects of Young Qihuang of National Administration of Traditional Chinese Medicine (2020).

Disclosure

The authors declare no conflict of interest, financial or otherwise.

References

1. Sung H, Ferlay J, Siegel RL, et al. Global cancer statistics 2020: GLOBOCAN estimates of incidence and mortality worldwide for 36 cancers in 185 countries. *Cancer J Clin.* 2021;71(3):209–249. doi:10.3322/caac.21660
2. Mehlen P, Puisieux A. Metastasis: a question of life or death. *Nat Rev Cancer.* 2006;6(6):449–458. doi:10.1038/nrc1886
3. Hejna M, Wöhrer S, Schmidinger M, Raderer M. Postoperative chemotherapy for gastric cancer. *Oncologist.* 2006;11(2):136–145. doi:10.1634/theoncologist.11-2-136
4. Hara H, Kadowaki S, Asayama M, et al. First-line bolus 5-fluorouracil plus leucovorin for peritoneally disseminated gastric cancer with massive ascites or inadequate oral intake. *Inter J Clin Oncol.* 2018;23(2):275–280. doi:10.1007/s10147-017-1198-7

5. Chen GQ, Nan Y, Huang SC, et al. Research progress of ginger in the treatment of gastrointestinal tumors. *World J Gastrointest Oncol.* 2023;15(11):1835–1851. doi:10.4251/wjgo.v15.i11.1835
6. Huang S, Wang L, Wang Z, et al. Multiomics strategy reveals the accumulation and biosynthesis of bitter components in *Zanthoxylum schinifolium* Sieb. *Food Res Intern.* 2022;162(Pt A):111964. doi:10.1016/j.foodres.2022.111964
7. Fu L, Xie H, Shi S. Multielement analysis of *Zanthoxylum bungeanum* maxim. *Essential Oil Using ICP-MS/MS Analytic Bioanalytic Chem.* 2018;410(16):3769–3778. doi:10.1007/s00216-018-1040-8
8. Ye N, Wang WS, Zhang HL, et al. Progress in the study of pharmacological effects of dried ginger and its medicinal pairs. *Chin J Trad Chin Med.* 1–14.
9. Uthaisaisangwong A, Oranratanaphan S, Musigavong N. Effects of ginger adjunct to the standard prophylaxis on reducing carboplatin and paclitaxel-induced nausea vomiting: a randomized controlled study. *Support Care Cancer.* 2020;28(8):3831–3838. doi:10.1007/s00520-019-05201-5
10. Yu YY, Zhu YJ, Xiao ZZ, et al. Effect of Zhi Mu and dried ginger on gefitinib resistance in non-small cell lung cancer mediated by abnormal activation of PI3K/AKT pathway and the mechanism. *New Chin Med Clin Pharmacol.* 2023;34(11):1525–1533.
11. Kiyama R. Nutritional implications of ginger: chemistry, biological activities and signaling pathways. *J Nutr Biochem.* 2020;86:108486. doi:10.1016/j.jnutbio.2020.108486
12. He HJ, Wang JX, Yang Y, et al. Dajianzhong Tang mediates ERK1/2 signaling pathway to regulate MMP-9 expression in an animal model of spleen-yang deficiency gastric cancer. *Chin Ethnic Folk Med.* 2017;26(22):24–27.
13. Liu J, Wang S, Zhang Y, Fan HT, Lin HS. Traditional Chinese medicine and cancer: history, present situation, and development. *Thoracic Cancer.* 2015;6(5):561–569. doi:10.1111/1759-7714.12270
14. Zhang Z, Shen P, Liu J, et al. In vivo study of the efficacy of the essential oil of *Zanthoxylum bungeanum* pericarp in dextran sulfate sodium-induced murine experimental colitis. *J AgriculFood Chem.* 2017;65(16):3311–3319. doi:10.1021/acs.jafc.7b01323
15. Yuan HM, Qiu L, Xie ZJ, Zou L, Zheng J, Fu Q. Research progress on alkaloids constituents from *Zanthoxylum* and their pharmacological activities. *Zhongguo Zhong yao za zhi.* 2015;40(23):4573–4584.
16. Tian YQ, Hu D, Zhang YL, Zou J, Chen GL, Guo MQ. Inhibitors targeting multiple janus kinases from *Zanthoxylum simulans* mediate inhibition and apoptosis against gastric cancer cells via the estrogen pathway. *Front Chem.* 2022;10:922110. doi:10.3389/fchem.2022.922110
17. Park YS, Nam GH, Jo KJ, Kawk HW, Kim SY, Kim YM. Extract from *Zanthoxylum piperitum* induces apoptosis of ags gastric cancer cells through Akt/MDM2/p53 signaling pathway. *Chin J Integr Med.* 2021;27(10):752–759. doi:10.1007/s11655-021-3486-8
18. Akimoto M, Iizuka M, Kanematsu R, Yoshida M, Takenaga K. Anticancer effect of ginger extract against pancreatic cancer cells mainly through reactive oxygen species-mediated autotic cell death. *PLoS One.* 2015;10(5):e0126605. doi:10.1371/journal.pone.0126605
19. Radhakrishnan EK, Bava SV, Narayanan SS, et al. [6]-Gingerol induces caspase-dependent apoptosis and prevents PMA-induced proliferation in colon cancer cells by inhibiting MAPK/AP-1 signaling. *PLoS One.* 2014;9(8):e104401. doi:10.1371/journal.pone.0104401
20. Mo Z, Xian Y, Zhang R, Dai Y, Chen W, Nie K. 6-Gingerol, a major ingredient of ginger, attenuated cisplatin-induced pica in rats via regulating 5-HT3R/Ca²⁺/CaMKII/ERK1/2 signaling pathway. *J Func Foods.* 2023;100:105389. doi:10.1016/j.jff.2022.105389
21. Wang X, Wang ZY, Zheng JH, Li S. TCM network pharmacology: a new trend towards combining computational, experimental and clinical approaches. *Chinese J Nat Med.* 2021;19(1):1–11. doi:10.1016/S1875-5364(21)60001-8
22. Lu D, Yuan L, Ma X, et al. The mechanism of polyphyllin in the treatment of gastric cancer was verified based on network pharmacology and experimental validation. *Heliyon.* 2024;10(10):e31452. doi:10.1016/j.heliyon.2024.e31452
23. Fan M, Jin C, Li D, et al. Multi-level advances in databases related to systems pharmacology in traditional Chinese medicine: a 60-year review. *Front Pharmacol.* 2023;14:1289901. doi:10.3389/fphar.2023.1289901
24. Jiang YL, Xun Y. Molecular mechanism of salvia miltiorrhiza in the treatment of colorectal cancer based on network pharmacology and molecular docking technology. *Drug Des Devel Ther.* 2024;18:425–441. doi:10.2147/DDDT.S443102
25. Zhang YQ, Li S. Some advances in network pharmacology and modern research of traditional Chinese medicine. *Chin J Pharmacol Toxicol.* 2015;29(06):883–892.
26. Yan Z, Lai Z, Lin J. Anticancer properties of traditional Chinese medicine. *Comb Chem High Throughput Screening.* 2017;20(5):423–429. doi:10.2174/1386207320666170116141818
27. Clough E, Barrett T. The gene expression omnibus database. *Methods Molecular Biol.* 2016;1418:93–110.
28. Lu DD, Yuan L, Wang ZZ, et al. To explore the mechanism of Yigong San anti-gastric cancer and immune regulation. *World J Gastrointest Oncol.* 2024;16(5):1965–1994. doi:10.4251/wjgo.v16.i5.1965
29. Zanotelli MR, Zhang J, Reinhart-King CA. Mechanoresponsive metabolism in cancer cell migration and metastasis. *Cell Metab.* 2021;33(7):1307–1321. doi:10.1016/j.cmet.2021.04.002
30. Bailly C. *Ruta angustifolia* pers. (Narrow-leaved fringed rue): pharmacological properties and phytochemical profile. *Plants.* 2023;12(4):827. doi:10.3390/plants12040827
31. Sandjo LP, Kuete V, Tchagna RS, Efferth T, Ngadjui BT. Cytotoxic Benzophenanthridine and Furoquinoline Alkaloids from *Zanthoxylum buesgenii* (Rutaceae). *Chem Cent J.* 2014;8(1):61. doi:10.1186/s13065-014-0061-4
32. Chen H, Li S, Wang S, Li W, Bao N, Ai W. The inhibitory effect of kokusaginine on the growth of human breast cancer cells and MDR-resistant cells is mediated by the inhibition of tubulin assembly. *Bioorg Med Chem Lett.* 2018;28(14):2490–2492. doi:10.1016/j.bmcl.2018.05.059
33. Huo CL, Wang B, Zhang X, Sun ZG. Skimmianine attenuates liver ischemia/reperfusion injury by regulating PI3K-AKT signaling pathway-mediated inflammation, apoptosis and oxidative stress. *Sci Rep.* 2023;13(1):18232. doi:10.1038/s41598-023-45354-2
34. Liu Y, Kang L, Shi SM, et al. Skimmianine as a novel therapeutic agent suppresses proliferation and migration of human esophageal squamous cell carcinoma via blocking the activation of ERK1/2. *Neoplasma.* 2022;69(3):571–582. doi:10.4149/neo_2022_211118N1640
35. Chan BC, Ip M, Gong H, et al. Synergistic effects of diosmetin with erythromycin against ABC transporter over-expressed methicillin-resistant *Staphylococcus aureus* (MRSA) RN4220/pUL5054 and inhibition of MRSA pyruvate kinase. *Phytomedicine.* 2013;20(7):611–614. doi:10.1016/j.phymed.2013.02.007
36. Chandler D, Woldu A, Rahmadi A, et al. Effects of plant-derived polyphenols on TNF-alpha and nitric oxide production induced by advanced glycation endproducts. *Mol Nutr Food Res.* 2010;54(Suppl 2):S141–150. doi:10.1002/mnfr.200900504

37. Liao W, Ning Z, Chen L, et al. Intracellular antioxidant detoxifying effects of diosmetin on 2,2-azobis(2-amidinopropane) dihydrochloride (AAPH)-induced oxidative stress through inhibition of reactive oxygen species generation. *J Agric Food Chem*. 2014;62(34):8648–8654. doi:10.1021/jf502359x
38. Zhang F, Luo H. Diosmetin inhibits the growth and invasion of gastric cancer by interfering with M2 phenotype macrophage polarization. *J Biochem Mol Toxicol*. 2023;37(10):e23431. doi:10.1002/jbt.23431
39. Koosha S, Mohamed Z, Sinniah A, Alshawsh MA. Investigation into the molecular mechanisms underlying the anti-proliferative and anti-tumorigenesis activities of diosmetin against HCT-116 human colorectal cancer. *Sci Rep*. 2019;9(1):5148. doi:10.1038/s41598-019-41685-1
40. Li H, Chen C. Quercetin has antimetastatic effects on gastric cancer cells via the interruption of uPA/uPAR function by modulating NF- κ B, ERK1/2, and AMPK α . *Integr Cancer Ther*. 2018;17(2):511–523. doi:10.1177/1534735417696702
41. Ji W, Liu W, Huo Y, Hu C, Zhang Y. Banxia Xiexin decoction ameliorates dextran sulfate sodium (DSS)-induced ulcerative colitis via inhibiting serine-threonine protein kinase (Akt)/mitogen-activated protein kinase (MAPK) signaling pathway. *Biotechnol Appl Biochem*. 2023;70(4):1530–1542. doi:10.1002/bab.2451
42. Zhang MM, Wang D, Lu F, et al. Identification of the active substances and mechanisms of ginger for the treatment of colon cancer based on network pharmacology and molecular docking. *BioData mining*. 2021;14(1):1. doi:10.1186/s13040-020-00232-9
43. Lurje G, Lenz HJ. EGFR signaling and drug discovery. *Oncology*. 2009;77(6):400–410. doi:10.1159/000279388
44. Wang BH, Qian W, Gao YJ, Wang HF, Hou XH. Effects of inhibition of cyclooxygenase-2 by RNA interference on proliferation and apoptosis of human gastric cancer cells: an experimental study with human gastric cancer cells and mice. *Zhonghua yi xue za zhi*. 2006;86(4):266–271.
45. Shi J, Lu Y, Wei P. Xiaotan Sanjie decoction inhibits angiogenesis in gastric cancer through interleukin-8-linked regulation of the vascular endothelial growth factor pathway. *J Ethnopharmacol*. 2016;189:230–237. doi:10.1016/j.jep.2016.05.043
46. Wan FS, Wu J, Li H, Tu S, Yu LH. Study on apoptosis of human stomach SGC-7901 cells induced by extracts of Solanum lyratum. *Zhong yao cai*. 2009;32(2):245–249.
47. Yang Q, Ye ZY, Zhang JX, Tao HQ, Li SG, Zhao ZS. Expression of matrix metalloproteinase-9 mRNA and vascular endothelial growth factor protein in gastric carcinoma and its relationship to its pathological features and prognosis. *Anatomic Record*. 2010;293(12):2012–2019. doi:10.1002/ar.21071
48. Li JX, Sun L, Zhao S, et al. Differences in clinicopathological features, gene mutations, and prognosis between primary gastric and intestinal gastrointestinal stromal tumors in 1061 patients. *Zhonghua wei Chang Wai Ke Za Zhi*. 2023;26(4):346–356. doi:10.3760/cma.j.cn441530-20220531-00234
49. Wu W, Wei N, Shao G, Jiang C, Zhang S, Wang L. circZNF609 promotes the proliferation and migration of gastric cancer by sponging miR-483-3p and regulating CDK6. *Onco Targets Ther*. 2019;12:8197–8205. doi:10.2147/OTT.S193031
50. Wan Y, Liu D, Xia J, et al. Ginsenoside CK, rather than Rb1, possesses potential chemopreventive activities in human gastric cancer via regulating PI3K/AKT/NF- κ B signal pathway. *Front Pharmacol*. 2022;13:977539. doi:10.3389/fphar.2022.977539
51. Li LP, Wu WJ, Sun DY, Xie ZY, Ma YC, Zhao YG. miR-449a and CDK6 in gastric carcinoma. *Oncol Lett*. 2014;8(4):1533–1538. doi:10.3892/ol.2014.2370

Drug Design, Development and Therapy

Publish your work in this journal

Drug Design, Development and Therapy is an international, peer-reviewed open-access journal that spans the spectrum of drug design and development through to clinical applications. Clinical outcomes, patient safety, and programs for the development and effective, safe, and sustained use of medicines are a feature of the journal, which has also been accepted for indexing on PubMed Central. The manuscript management system is completely online and includes a very quick and fair peer-review system, which is all easy to use. Visit <http://www.dovepress.com/testimonials.php> to read real quotes from published authors.

Submit your manuscript here: <https://www.dovepress.com/drug-design-development-and-therapy-journal>

Dovepress
Taylor & Francis Group